A bioactive three-layered skin substitute based on ECM components effectively promotes skin wound healing and regeneration

Carlos Chocarro-Wrona [a,b,c,d,e,1], Paula Pleguezuelos-Beltrán [a,b,c,d,e,1],
Julia López de Andrés [a,b,c,d,e], Cristina Antich [a,b,d,e,f], Juan de Vicente [d,g],
Gema Jiménez [a,b,c,d,e], Salvador Arias-Santiago [b,h,i], Patricia Gálvez-Martín [j,*],
Elena López-Ruiz [a,b,d,e,k,**], Juan Antonio Marchal [a,b,c,d,e,***]

[a] Biopathology and Regenerative Medicine Institute (IBIMER), Center for Biomedical Research (CIBM), University of Granada, 18016, Granada, Spain
[b] Instituto de Investigación Biosanitaria ibs.GRANADA, University Hospitals of Granada, University of Granada, 18012, Granada, Spain
[c] Department of Human Anatomy and Embryology, Faculty of Medicine, University of Granada, 18016, Granada, Spain
[d] Excellence Research Unit "Modelling Nature" (MNat), University of Granada, 18016, Granada, Spain
[e] BioFab i3D - Biofabrication and 3D (bio)printing laboratory, University of Granada, 18016, Granada, Spain
[f] National Center for Advancing Translational Sciences, National Institute of Health, 28050, Rockville, MD, USA
[g] F2N2Lab, Magnetic Soft Matter Group, Department of Applied Physics, Faculty of Sciences, University of Granada, 18071, Granada, Spain
[h] Dermatology Department, Hospital Universitario Virgen de las Nieves, 18012, Granada, Spain
[i] Dermatology Department, Faculty of Medicine, University of Granada, 18016, Granada, Spain
[j] R&D Animal and Human Health, Bioibérica S.A.U, 08950, Barcelona, Spain
[k] Department of Health Sciences, University of Jaén, 23071, Jaén, Spain

A R T I C L E I N F O

A B S T R A C T

To overcome the limitations of conventional skin tissue engineering (TE), 3D biofabrication approaches are being developed. However, tissue mimicry should be further improved in skin models. Here, we developed and characterized biomimetic hydrogels to obtain a biofabricated three-layered (BT) skin substitute based on the main components found in the epidermal, dermal, and hypodermal skin layers. Hydrogels for dermal and hypodermal skin layers were based on a mix of agarose and type I collagen, supplemented with skin-related extracellular matrix (ECM) components (dermatan sulfate, hyaluronic acid, and elastin) and loaded with human dermal fibroblasts (hDFs) or human mesenchymal stem/stromal cells (hMSCs), respectively. The epidermal hydrogel was formulated using type I collagen supplemented with keratin and sphingolipids, and seeded with human epidermal keratinocytes (hEKs). Physicochemical results revealed adequate viscosity, gelling times, and pH for each hydrogel solution. The BT Skin also showed good swelling and degradation kinetics, and mechanical properties in a similar range of human skin. The hydrogels and BT Skin demonstrated stable cell viability and metabolic activity, as well as intercellular communication through the release of growth factors. Moreover, the BT Skin demonstrated controlled inflammation *in vivo*, and produced results comparable to autografting in a mouse skin wound model. This bioactive and biomimetic three-layered BT Skin has a composition that attempts to mimic the natural ECM of the skin, formulated with the characteristic cells and biomolecules present in each skin layer, and offers promising properties for its clinical application in the treatment of patients with skin injuries.

---

1. Introduction

The skin, one of the largest organs of the body, plays paramount roles in protecting inner organs from physical, chemical, and biological hazards, and is also involved in preventing excessive transepidermal water loss (TEWL), thermoregulation, sensorial perception, or excretion [1–4]. In addition, the skin also synthesizes, processes, and metabolizes a wide range of proteins, glycosaminoglycans (GAGs), lipids, and signaling molecules [5]. Skin substitutes, typically manufactured by tissue engineering (TE), are an important field of research with great impact on dermatological pathology treatments. They should show biocompatible properties, help to restore the epidermal barrier function and cutaneous homeostasis (temperature, pH, TEWL, elasticity, and moisture), and ensure a correct clinical outcome [6–8]. Currently, there are very few skin substitutes that meet all of these requirements, and the available models only comprise one or two-layered tissues. In addition, most substitutes are predominantly acellular or only contain one or two types of cells [9]. However, the skin is structured in three main layers. The outermost layer of the skin is the epidermis, which provides a waterproof barrier. The epidermis mainly consists of layers of keratinocytes that produce keratin, the primary structural protein of this layer [10]. Sphingolipids are also bioactive molecules present in the epidermis that contribute to the maintenance of the skin barrier [11]. The dermis, which is beneath the epidermis, is composed of connective tissue mainly consisting of collagen, elastin, and GAGs. Fibroblasts, the primary cell type of the dermis, produce extracellular matrix (ECM) components, growth factors, and enzymes that remodel the skin and support keratinocyte proliferation and differentiation [12]. The deeper subcutaneous tissue is the hypodermis, made up of fat and connective tissue. It protects the internal tissues and organs from cold and trauma, provides energy, and participates in hormone synthesis. This layer is crucial for maintaining the skin's mechanical and thermoregulatory properties [10]. Therefore, one of the challenges in developing skin substitutes is to fabricate a multilayered scaffold that mimics the natural skin tissue.

Many TE skin products currently on the market have demonstrated that using structural proteins can increase the rate of wound healing [13]. Engineering bioactive scaffolds based on components such as collagen-hyaluronic acid (HA) hydrogels [14], collagen-elastin-HA scaffolds [15], collagen/GAGs-based matrices [16], or hybrid plasma-elastin hydrogels [17,18], has emerged as a promising alternative to treat skin injuries. However, while the dermis and epidermis have been extensively studied, the hypodermis is often not included. Despite its essential role in regulating the upper dermal and epidermal layers by supporting the proliferation of keratinocytes and fibroblasts, few studies have incorporated the hypodermis into TE skin substitutes [19–24]. With the hypothesis that a skin substitute capable of better replicating the composition and hierarchical structure of natural skin tissue, currently absent in skin TE substitutes, could be developed, our laboratory has biofabricated three biologically-inspired hydrogels, each one designed to closely resemble the ECM found in each skin layer.

Collagen is the major ECM protein of the skin and is predominantly located in the dermis, providing mechanical strength and structural integrity. Moreover, collagen I influences skin cell functions and the synthesis of ECM proteins [25,26]. For keratinocytes, collagen provides a structural scaffold that supports their growth, proliferation, and differentiation, which is crucial for maintaining skin integrity and wound healing [27]. As a result, collagen I is a preferred material for skin scaffolds due to its ability to enhance the formation of functional skin tissues [25]. Therefore, the epidermal hydrogel was based on type I collagen as a scaffolding biomaterial, supplemented with keratin, due to its presence in epithelial tissues, where it provides mechanical support and external resistance [28,29], and sphingolipids, which contribute to the maintenance of the epidermal barrier against desiccation and penetration of xenobiotics [30]. Regarding the cellular fraction, the epidermal layer was populated with epidermal keratinocytes (hEKs), as these are the most representative cell type in the epidermis.

Considering the limited mechanical strength of collagen-based hydrogels for skin TE applications, collagen is often blended with natural and synthetic polymers [26]. In this study, the dermal and hypodermal hydrogels were based on collagen I and agarose, a biocompatible polymer which provides enhanced mechanical support and fast gelation [31,32] compared to collagen I, which contributes with slower gelation and supports cellular growth, facilitating the development of functional skin [33]. Both materials were supplemented with a blend of dermatan sulfate, a highly relevant glycan in skin ECM that participates in its reconstruction during the wound healing process [34–36], and HA, which is the main GAG found in the dermal ECM. HA is commonly used in skin care products and TE, promoting wound healing, skin moisture maintenance, and cell proliferation [37–41]. Moreover, for the dermal hydrogel, the combination of agarose/collagen I-based hydrogel with dermatan sulfate and HA was also supplemented with elastin, the main constituent of elastic fibers, which comprises 2–4% of the total dry weight of the dermis. By incorporating natural polymers like elastin, hydrogels can mimic the elastic ECM composition of the skin and obtain better mechanical properties [18,42,43].

The dermal hydrogel was populated with dermal fibroblasts (hDFs), as they play a vital role in skin remodeling and wound healing [42,43]. For the hypodermal layer, human adipose-derived mesenchymal stem/stromal cells (hMSCs) were used, as they can promote wound healing and have been described to migrate to the wound site, differentiate, and repopulate the injured tissue by promoting regeneration [44].

Consequently, the main objective of this study was to develop and characterize bioactive and biomimetic hydrogels for fabricating a skin substitute with epidermal, dermal, and hypodermal layers for skin TE. After evaluating the diverse physicochemical, mechanical, and biological properties of the hydrogel solutions, we biofabricated a three-layered (BT) skin substitute that was characterized *in vitro*. Further, the BT Skin substitute was transplanted onto the back of immunodeficient mice, and its full-thickness skin wound healing properties were assessed.

2. Materials and methods

2.1. Materials

Collagen type I (3.3 mg/mL rat tail collagen I, 354236) was purchased from Corning®; marine-derived keratin (Kerapro S) from Proalan S.A. (Barcelona, Spain); animal-derived sphingolipids, dermatan sulfate, and HA, from Bioibérica S.A.U. (Barcelona, Spain); and elastin (E6527) and NaHCO$_3$ (S5761) from Sigma (St. Louis, MO, USA). Dulbecco's Modified Eagle's Medium (DMEM, 31966021), Penicillin and streptomycin (P/S, 10.000 U/ml, 15140122), and fetal bovine serum (FBS, 10270106) were obtained from Gibco. Agarose (UltraPure™ Low Melting Point Agarose, 16520100), AlamarBlue HS® (A50101), LIVE/DEAD™ Viability/Cytotoxicity Kit (L3224), CellTracker™ Green CMFDA (C2925), CellTracker™ Red CMTPX (C34552), Hoechst (H21486), Cytokeratin Pan antibody (PA1-27114), and Alexa Fluor-488-conjugated anti-rabbit antibody (A-11008) were purchased from Invitrogen (Massachusetts, EEUU). PE anti-human HLA-A,B,C (311406), APC anti-mouse H-2Kd (116620), and PE Mouse IgG2a, κ Isotype Ctrl (400213) antibodies were obtained from Biolegend; CD31-APC antibody (130-111-541) from Miltenyi Biotec; and PPARγ antibody (16643-1-AP) from Proteintech. Fibronectin (ab2413), VEGFA (ab52917), and VE-Cadherin (ab33168) antibodies, Mouse Inflammation Antibody Array - Membrane (40 Targets; ab133999), and Human Growth Factor Antibody Array - Membrane (41 Targets; ab134002) were obtained from Abcam. Phosphate-buffered saline (PBS) was bought from Medicago AB (Uppsala, Sweden); 0.22 μm membrane filters from Merck Millipore; Optimal Cutting Temperature (OCT) compound (Tissue-Tek®) from Sakura Finetek; Mupirocin antibiotic ointment (20 mg/g) from ISDIN; Bupredine analgesic (0.3 mg/mL, 10 mL) from Fatro Ibérica, Desvern

(Barcelona, Spain), Ganadexil Enrofloxacin antibiotic (5 %, 100 mL) from Industrial Veterinaria, S.A. Invesa; and 1,4-butanediol thermoplastic polyurethane elastomer (b-TPUe) from Recreus Industries S.L. (Spain).

2.2. Cell culture

The human skin samples with subcutaneous adipose tissue were transported to the laboratory in DMEM with 1 % P/S. hMSCs were isolated from the subcutaneous adipose tissue and characterized as previously reported [45,46], while hDFs and hEKs were respectively isolated from the dermis and epidermis of the skin samples, as previously described [47]. All human samples used in this study were obtained after informed consent and authorization was provided from the

Granada Provincial Ethics Committee (Ministry of Health and Families, Andalusia, Spain, reference: 0467-N-20). Once isolated, hMSCs and hDFs were cultured in high-glucose DMEM supplemented with 10 % FBS and 1 % P/S, while hEKs were cultured in keratinocyte medium as previously reported [47]. Cells were cultured at 37 °C in a humidified atmosphere containing 5 % CO_2. The medium was refreshed every 3 days. At 80 % of confluence, cells were passaged and embedded in the hydrogels.

2.3. Hydrogel solutions and BT skin preparation

Firstly, a 3 % (w/v) agarose solution was prepared in PBS, autoclaved at 120 °C for 2 h, and stored at 4 °C until use. Agarose was preheated and maintained at 37 °C in a water bath to avoid gelation and
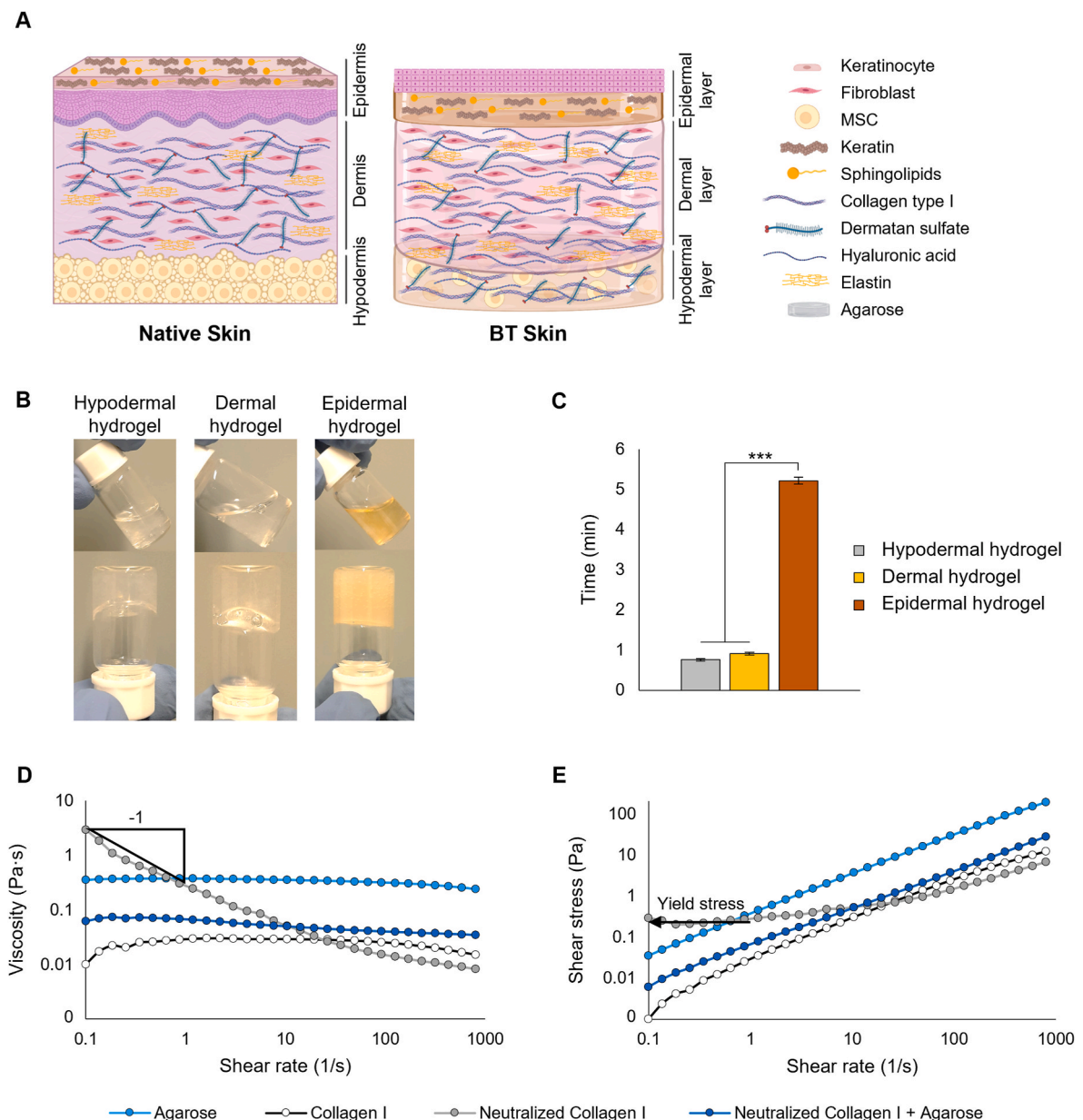

Fig. 1. (A) Design of the BT Skin substitute, with its different components, compared with native skin. (B) Tube inversion test images. (C) Time of tube inversion for each hydrogel: hypodermal, dermal, and epidermal. Statistical analysis was performed using Brown-Forsythe and Welch ANOVA tests, followed by Tamhane T2 post-hoc test for multiple comparisons. Statistical significance: ***P < 0.005. (D) Viscosity curves and (E) rheograms (shear stress vs shear rate) of the main components of the hydrogels (Agarose, Collagen I, neutralized Collagen I, and neutralized Collagen I + Agarose). The yielding behavior of neutralized Collagen I is demonstrated by both the slope of −1 on the triangle and the horizontal arrow in figures (D) and (E), respectively. Fig. (A) created with BioRender.com. (For interpretation of the references to color in this figure legend, the reader is referred to the Web version of this article.)

stabilize its temperature at 37 °C. A 3.3 mg/mL collagen I solution, previously syringe-sterilized using filters of 0.22 μm pore size, was neutralized with 0.8 M NaHCO$_3$ (adding 70 μL per mL of collagen I solution). Then, three solutions using keratin, sphingolipids, dermatan sulfate, HA, and elastin diluted in PBS were prepared: i) keratin + sphingolipids; ii) dermatan sulfate + HA; and iii) dermatan sulfate + HA + elastin. Each solution was mixed with the collagen I solution to obtain the final concentrations shown in Table S1. All component solutions were syringe-sterilized through a 0.22 μm membrane before their use.

To biofabricate the BT Skin, cell-loaded dermal and hypodermal hydrogel solutions were prepared by mixing [collagen I + dermatan sulfate/HA/elastin] with hDFs, and [collagen I + dermatan sulfate/HA] with hMSCs, respectively. Then, pre-heated agarose was added to each blend, obtaining a final concentration of 1·10^6 cells/mL. First, the hypodermal solution mix ([collagen I + dermatan sulfate/HA] + hMSCs + agarose) was poured into well plates and allowed to gel for 5 min. Then, the dermal layer blend ([collagen I + dermatan sulfate/HA/elastin] + hDFs + agarose) was poured onto the hypodermal layer and let to gel. Once both hypodermal and dermal layers were obtained, the epidermal hydrogel solution [collagen I + keratin/sphingolipids] was laid on top and allowed to gel inside an incubator at 37 °C for 15 min. Once the epidermal layer gelled, 2·10^6 hEKs were seeded on top of the BT Skin hydrogel and cultured for 1 week (Fig. 1A). After this time, samples were partially dehydrated by the application of 100 g of pressure for 2 min, giving the hydrogels a higher resistance and enhancing their stiffness and mechanical properties [43,48,49]. BT Skin hydrogels were cultured in keratinocyte medium for the first 2–3 days to ensure hEKs attachment to the surface of the epidermal layer. Afterward, the medium was replaced with DMEM for the following days.

2.4. Physicochemical characterization of the hydrogel solutions

2.4.1. Macroscopic characteristics
The physical appearance of the hydrogel solutions was inspected visually. Macroscopic aspects, turbidity, and color were also evaluated.

2.4.2. Tube inversion test
The tube inversion test was used to define the gelation time of the hydrogels. The liquid hydrogel solutions were poured into glass vials, inverting the vials upside down every 1 min to check the formation of stable gels. The gelation time was estimated as the time point when the samples formed a stable, solid gel that remained at the bottom of the vials when inverted.

2.4.3. Rheological characterization
The rheological characterization of the main components of the hydrogel solutions was carried out with a torsional rheometer MCR302 (Anton Paar, Austria). The shear viscosity was obtained at 37 °C using a concentric cylinder system. First, the hydrogel solution samples were placed inside the cup and pre-sheared at a constant shear rate of 500 s^{-1} for 1 min to remove the mechanical history of the sample. Then, the sample was allowed to rest for 1 min, with no shear rate applied. Lastly, the bob was rotated at increasing angular velocities to measure the torque exerted by the sample. The shear rate was logarithmically ramped from 0.01 to 800 s^{-1} for 2.5 min and the data acquisition time was 5 s. All experiments were run in triplicates.

2.5. Physicochemical characterization of the BT skin

2.5.1. pH determination
The pH of the BT Skin hydrogel was determined using a calibrated digital pH meter Hach Sension$^+$ (Hach Lange S.L., Spain) at room temperature (RT).

2.5.2. Swelling test
Swelling rates of freeze-dried samples were determined as previously

described [50]. Briefly, samples were pre-weighed and submerged in PBS. The swelling rate of the BT Skin was calculated at different time points as follows:

$$Swelling\ ratio\ (\%) = \left(\frac{(W_t - W_0)}{W_0}\right) x\ 100$$

W_0 represents the initial weight of samples at day zero and W_t represents the wet weight of samples at the corresponding time point.

2.5.3. Degradation test
The degradation rate was analyzed by quantifying the weight loss of samples over time. The BT Skin was incubated under gentle agitation at 37 °C, retrieved at different time points, and centrifuged at 5000 rpm for 2 min. Supernatant was removed, and samples were weighed [50]. Degradation rate (%) was calculated as a measure of weight loss as follows:

$$Degradation\ ratio\ (\%) = \left(\frac{(W_i - W_t)}{W_i}\right) x\ 100$$

W_i represents the initial weight of samples and W_t represents the wet weight of hydrogels at the corresponding time point.

2.5.4. Mechanical analysis
The mechanical properties of the cell-free and cell-loaded BT Skin hydrogels before (Pre Cell-free BT Skin and Pre BT Skin) and after (Cell-free BT Skin and BT Skin) partial dehydration, maintained for 21 days, were evaluated using a torsional rheometer MCR302 in plate-plate configuration, and compared to abdominal full-thickness human skin biopsies. BT Skin samples were cast in a 20 mm diameter and 5 mm height mold to fit within the rheometer's plates. A three-step assay was designed to obtain both compression and shearing characteristics of hydrogels in one single experiment using the same sample. In the first step, the cylindrical sample was placed on the base of the rheometer and gently squeezed at a constant approaching velocity of 10 μm/s up to a normal force of 0.5 N. Secondly, the normal force was kept constant at 0.5 N for 30 s for stabilization. Thirdly, still under a 0.5 N load, the sample was oscillatory sheared with a logarithmically increasing strain amplitude from 0.001 % to 1000 % at a strain frequency of 1 Hz to measure the shear viscoelastic moduli. All experiments were run in triplicates.

2.6. Biological characterization of the hydrogels and BT skin

2.6.1. Cell viability assay
The LIVE/DEAD™ Viability/Cytotoxicity Kit was used to analyze cell viability. Separated hydrogels for hypodermal and dermal layers, seeded with hMSCs and hDFs, respectively, and BT Skin, seeded with hMSCs, hDFs, and hEKs in each respective layer, were stained using a calcein AM (2 μM; green) and ethidium homodimer (4 μM; red) solution diluted in PBS at 37 °C for 30 min. Samples were observed using confocal microscopy (Nikon Eclipse Ti-E A1, Nikon Instruments Europe B.V., Amsterdam Netherlands) at different times and analyzed using NIS-Elements software. Live and dead cells were quantified using the ImageJ (Fiji) software [51], determining the cell viability percentage as follows:

$$Cell\ viability\ (\%) = \frac{Live\ cells}{(Live\ cells + Dead\ cells)}\ x\ 100$$

2.6.2. Cell metabolic activity assay
The AlamarBlue HS® assay was used to analyze the cell metabolic activity of the samples after 0, 1, 3, 5, 7, 14, and 21 days of culture. Separated hydrogels for hypodermal and dermal layers, seeded with hMSCs and hDFs, respectively, and BT Skin, seeded with hMSCs, hDFs, and hEKs in each respective layer, were incubated with the AlamarBlue HS® solution at 37 °C for 1 h. The fluorescence of the reduced solution after incubation was determined at 530/590 nm excitation/emission

wavelengths in a Synergy® HT multidetection microplate reader (Bio-Tek Instruments, Inc., Winooski, VT, USA).

2.6.3. Cell distribution in the BT skin

To observe the distribution of the three cell types within each layer of the BT Skin hydrogel, hMSCs, hDFs, and hEKs were harvested by trypsinization, centrifuged, and stained with CellTracker™ Green CMFDA, CellTracker™ Red CMTPX, and CellTracker™ Green CMFDA, respectively, following manufacturer's instructions. Stained cells were loaded in their respective hydrogel solution and the BT Skin was prepared as previously described. Images of the distribution of the three differentiated layers were taken after 21 days in culture with a Nikon Eclipse Ti-E A1 confocal microscope and analyzed with NIS-Elements software.

2.6.4. Growth factors array

The release of different human growth factors was assessed by analyzing the conditioned media collected after culturing the BT Skin for 3 and 21 days, using the Human Growth Factor Antibody Array – Membrane according to the manufacturer's recommendations. Briefly, the membrane array was incubated in blocking buffer solution for 30 min. The conditioned media was added to the membrane and incubated at RT for 2 h. After multiple washes, the membrane array was incubated with 1 mL of biotin solution at RT for 2 h and washed again. The membrane array was subsequently incubated with 1 mL of streptavidin solution for 2 h at RT. Finally, detection buffer solution was added and membrane arrays were visualized using ChemiDoc MP Imaging System (BioRad).

2.7. In vivo assay

2.7.1. Wound healing animal model, surgical procedures, and experimental groups

A total of 32 ATHYM-Foxn1nu/nu male and female, immunodeficient, athymic, nude, and albino mice of 4 weeks of life (Janvier Labs, Le Genest-Saint-Isle, France), were employed for the *in vivo* assay. The mice were distributed randomly into the experimental groups, ensuring an equal number of males and females (4 females and 4 males per group). All animal handling procedures followed the national and European Union legislation (Spanish RD 53/2013 and EU Directive 2010/63) for the protection of animals used for scientific purposes and following the Ethical Principles and Guidelines for the Use of Animals approved by Provincial Ethics Committees of Granada (reference number: 1/062022/081).

Surgery to remove a skin area of 2 cm^2 from the upper dorsal, in a longitudinal position to the mouse spine, was performed using surgical scissors. A 3D-printed sterile, donut-shaped, porous b-TPUe [52] splint designed with a hinged lid (Fig. S1) was centered over the wound and secured with seven interrupted sutures [53]. Then, mice were transplanted with a BT Skin, a Cell-free BT Skin, and a skin autograft from the lower back (Autograft), or were left untreated as a control condition (Control) (n = 8 per group). Finally, the splint lid was closed with eight interrupted sutures.

For all groups, samples and splints were grafted, and an antibiotic ointment was applied. Also, an analgesic and an antibiotic were subcutaneously injected as postoperative treatment.

2.7.2. Skin repair monitoring

Throughout 8 weeks, a follow-up was carried out to collect clinical information, such as scar/wound area, and several homeostasis parameters. Scars were evaluated after 8 weeks using an adaptation of the Patient and Observer Scar Assessment Scale (POSAS) scale [54,55]. Every 2 weeks, mice were anesthetized using isoflurane inhalation to avoid unnecessary stress, and homeostasis skin parameters were measured using the Microcaya probe system (Microcaya S.L., Bilbao, Spain), comparing values of wounds/scars with a healthy area of skin (native skin) from each mouse of the study: the Thermometer® probe

allowed to measure skin temperature in °C; the Skin pH-meter® probe measured the skin pH; the Tewameter® probe determined the TEWL, as the evaporation of water in g/h/m^2; the Cutometer® probe analyzed the skin elasticity (μm) with suction (450 mbar of negative pressure – 2 s); the Corneometer® probe determined the skin moisturization through the capacitance of a dielectric medium; and the Mexameter® probe, based on the light absorption/reflection of three wavelengths, was able to measure the erythema and pigmentation of the skin, obtaining indirect information about the vascularization (hemoglobin levels) and pigmentation (melanin), respectively.

2.7.3. Histological and immunofluorescence analysis

Four and eight weeks after the surgical procedure, half of the mice were sacrificed at each time point, selected randomly while maintaining an equal number of males and females (two females and two males per group). Mice were sacrificed by cervical dislocation once anesthetized by isoflurane inhalation. Graft biopsies and native skin samples were collected, fixed in 4 % paraformaldehyde, dehydrated, embedded in paraffin or OCT compound, and cut into 5 μm or 8 μm sections using a microtome and a cryostat, respectively.

Paraffin sections were deparaffinized, rehydrated, and stained with Hematoxylin & Eosin (H&E) and Masson's Trichrome to reveal the histological structure. For immunofluorescence analysis, cryosections were incubated with primary antibodies against fibronectin, cytokeratin, PPARγ, VE-Cadherin, and VEGFA, followed by incubation with a secondary Alexa-488-conjugated anti-rabbit antibody. Additionally, other cryosections were stained with PE-conjugated anti-human HLA-A, B,C, APC-conjugated anti-mouse H-2Kd (MHC class I), PE-conjugated anti-mouse IgG2a, κ (isotype control), and APC-conjugated anti-mouse CD31, which did not require a secondary antibody. Finally, sections were counterstained with Hoechst, and images were obtained using a Leica DMi8 microscope.

2.7.4. Inflammation assessment

To assess the cytokine profile of the potential immune responses elicited by the biomaterials of the BT Skin substitute, 8 CD-1 immunocompetent female mice were used. The mice were randomly divided into two groups: a Cell-free BT Skin group (n = 4) and a control group (n = 4).

Mice were anesthetized using isoflurane inhalation, and a small incision was made on the dorsal skin using surgical scissors. In the Cell-free BT Skin group, BT Skin hydrogels without cells were implanted subcutaneously by gently positioning the material under the skin through the incision. For the control group, the same procedure was performed, but no hydrogel was implanted. In both groups, the wound was closed with interrupted sutures to ensure proper healing. All mice were subcutaneously injected with an analgesic solution for 3 days to avoid pain.

Two weeks after the implantation, mice were anesthetized, and blood was collected using sterile syringes *via* cardiac puncture which was immediately transferred into citrate-coated tubes to prevent coagulation. Following blood collection, the animals were humanely euthanized by cervical dislocation, in compliance with institutional ethical guidelines and approved protocols. Blood was centrifuged at 2000 rpm for 15 min at 4 °C to obtain plasma, which was stored at −80 °C. Plasma was analyzed with a mouse inflammation antibody dot blot array membrane, following the manufacturer's protocol. Finally, chemiluminescence signals were detected using a ChemiDoc MP Imaging System (BIO-RAD).

2.8. Statistical analysis

Results in this work are represented as mean ± standard deviation (SD). Statistical calculations were performed using GraphPad Prism 8.0.1 software. Data were analyzed using parametric or non-parametric tests depending on the distribution and homogeneity of variances, as

assessed by the Shapiro-Wilk and Brown-Forsythe tests, respectively. For comparisons between groups, one-way or two-way ANOVA tests, or mixed-effects model with the Geisser-Greenhouse correction, were performed with appropriate post-hoc analyses (e.g., Tukey, Dunnett, or Tamhane T2) for multiple comparisons. Non-parametric tests, such as Kruskal-Wallis with Dunn's post-hoc test, were applied where data did not meet normality or homoscedasticity assumptions. Specific tests for each experiment are detailed in the figure legends. Differences were considered statistically significant at P < 0.05 (*/#), P < 0.01 (**/##) and P < 0.005 (***/###).

3. Results

3.1. Physicochemical properties of hydrogels

3.1.1. Macroscopic characteristics

Fig. 1B shows the three hydrogels in their liquid state. Both hypodermal and dermal hydrogel solutions presented a whitish nearly transparent aspect, while the epidermal hydrogel solution showed a brownish color, quite turbid, due to its keratin component.

3.1.2. Tube inversion test

The gelling time was monitored by applying the tube inversion test for each hydrogel solution. Fig. 1B shows representative images of the hydrogels in their liquid and gel form. The average gelling times of the hypodermal, dermal, and epidermal hydrogels were 0.76 ± 0.03, 0.91 ± 0.03, and 5.22 ± 0.09 min (Fig. 1C), respectively.

3.1.3. Rheological characterization

Steady shear flow tests were carried out at 37 °C to measure the viscosity and yield stress of the major components of the hydrogels. Agarose and Collagen I solutions, as well as the Neutralized Collagen I + Agarose blend, demonstrated a Newtonian behavior, with a constant viscosity independent of the shear rate, obtaining results of 0.3492 ± 0.0178, 0.02859 ± 0.0013, and 0.0508 ± 0.0081 Pa·s, respectively. On the other hand, Neutralized Collagen I showed a shear-thinning behavior, with decreasing viscosity as shear rates increase (ranging from 0.2435 Pa·s at $\dot{\gamma} = 1.19$ s^{-1}, to 0.0153 Pa·s at $\dot{\gamma} = 91.4$ s^{-1}) (Fig. 1D). Moreover, whereas Agarose, Collagen I, and Neutralized Collagen I + Agarose blend lack yield stress, Neutralized Collagen I exhibited a plastic behavior manifested in Fig. 1E by the appearance of a yield stress of 0.3258 ± 0.1085 Pa. The yield stress is the minimum stress level that has to be overcome for the solution to flow.

3.2. Physicochemical properties of the BT skin

3.2.1. Macroscopic characteristics

Fig. 2A shows the macroscopic aspect of the BT Skin (black arrow signaling the epidermal layer). As can be observed, two main sections are visually differentiated: a) the upper opaque epidermal layer, made of collagen I with keratin and sphingolipids supplementation, with hEKs seeded on top; and b) the lower double dermal and hypodermal layers made of the blend of collagen I and agarose, supplemented with dermatan sulfate/HA/elastin and dermatan sulfate/HA, respectively. Both the hypodermal and dermal layers showed a translucid whitish shade, undifferentiated from each other. Fig. 2B and C shows the height
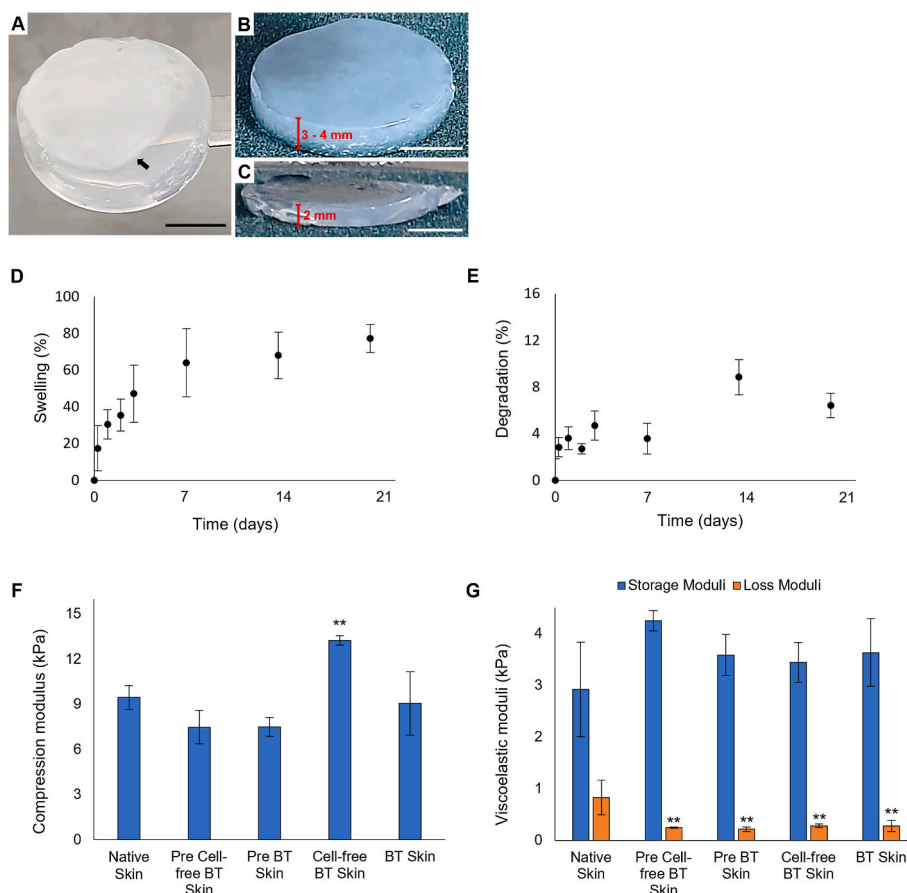

Fig. 2. (A) Macroscopic images of the BT Skin hydrogel (black arrow: epidermal layer), (B) before and (C) after partial dehydration (Scale bars = 5 mm). (D) Swelling behavior and (E) degradation percentage of BT Skin hydrogel over 21 days. (F) Compression moduli and (G) viscoelastic moduli of BT Skin hydrogels, with or without cells, before and after the partial dehydration process, after 21 days in culture, compared with human Native Skin. Statistical analysis was performed using the one-way ANOVA test, followed by Dunnett's post-hoc test for multiple comparisons against Native Skin. Statistical significance: **P < 0.01.

difference of the hydrogel before and after the partial dehydration process, where 2 mm of the hydrogel's height is reduced.

3.2.2. pH, swelling, and degradation performance of BT skin

The pH value of the full BT Skin hydrogel was 7.5 ± 0.1. The swelling kinetics of the freeze-dried BT Skin for 21 days are shown in Fig. 2D. The average swelling was 70 ± 7 %, reaching a plateau stage after 7 days. A degradation assay was carried out to analyze the endurance over time (Fig. 2E), showing a maximum of 8.8 ± 1.5 % mass loss after 14 days.

3.2.3. Rheological behavior of the BT skin

The compression moduli of the cell-free and cell-loaded BT Skin hydrogels before (Pre Cell-free BT Skin and Pre BT Skin) and after (Cell-free BT Skin and BT Skin) partial dehydration, maintained up to 21 days, and compared to human native skin biopsies, are depicted in Fig. 2F and Table S2. Even though variations were found in Cell-free BT Skin (13.25 ± 0.31 kPa) compared to native skin (9.46 ± 0.79 kPa), Pre Cell-free BT Skin (7.48 ± 1.11 kPa), Pre BT Skin (7.49 ± 0.63 kPa), and BT Skin (9.07 ± 2.11 kPa) showed no significant differences in comparison with the target tissue.

The viscoelastic moduli of cell-free and cell-loaded BT Skin hydrogels before and after dehydration are shown in Fig. 2G–Table S2, and Fig. S2. Although the four tested conditions showed the same storage modulus range of the native skin (2.92 ± 0.91 kPa), their loss moduli showed significant differences compared to the native skin loss modulus (0.83 ± 0.34 kPa).

3.3. Biological characterization of the hydrogels and BT skin

Biological characterization of the hypodermal and dermal hydrogels was carried out with cell viability and metabolic activity assays. Since the epidermal hydrogel was tricky to manipulate, as it showed to be flaccid once gelled, this hydrogel was incorporated into the BT Skin when the biological characterization of the full skin substitute was carried out. Cell metabolic activity of both hypodermal and dermal hydrogels at days 0, 1, 3, 5, 7, 14, and 21 is shown in Fig. 3A and C, respectively. Hypodermal hydrogels showed an increase in metabolic activity at day 5, maintaining a plateau stage until the end of the
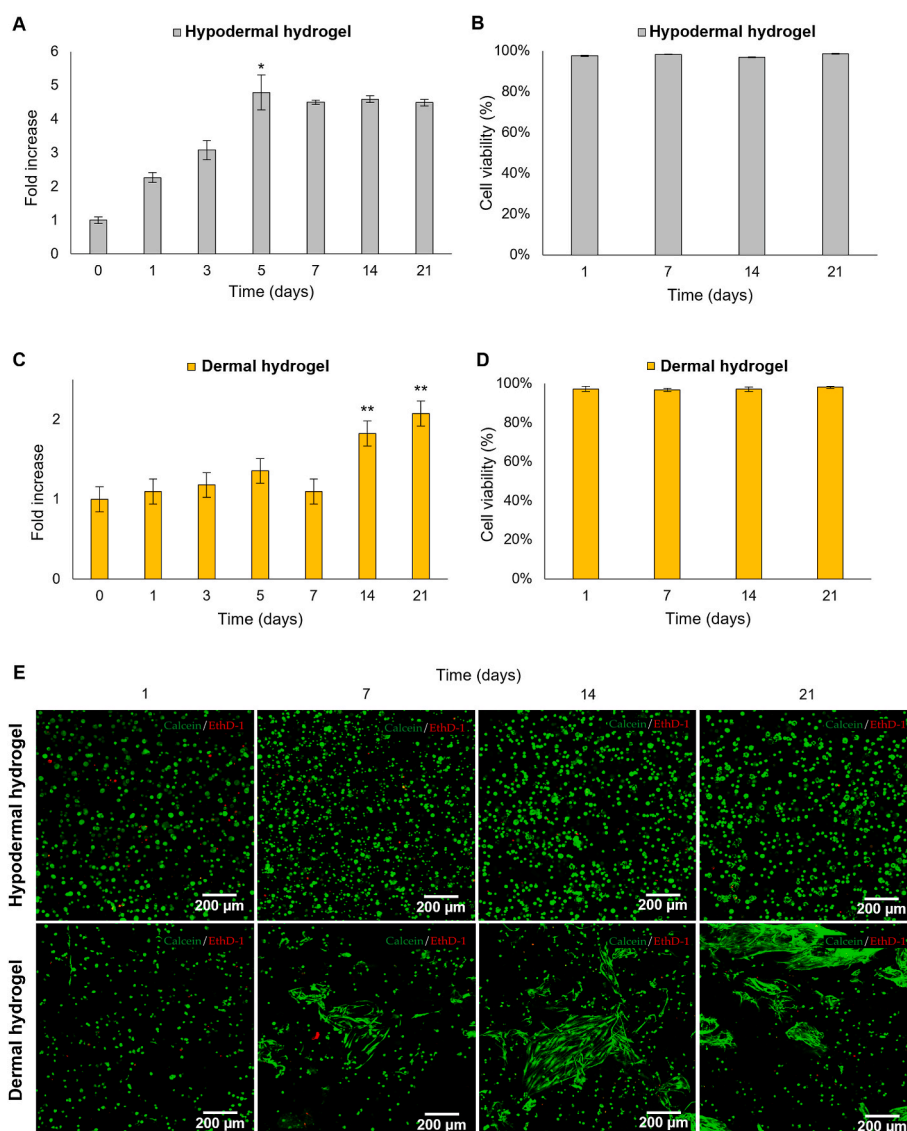

Fig. 3. Hypodermal hydrogel (A) cell metabolic activity at 0, 1, 3, 5, 7, 14, and 21 days, and (B) viability at 1, 7, 14, and 21 days. Dermal hydrogel (C) cell metabolic activity at 0, 1, 3, 5, 7, 14, and 21 days, and (D) viability at 1, 7, 14, and 21 days. (E) Representative confocal images of hypodermal and dermal hydrogels at days 1, 7, 14, and 21, showing live cells in green, and dead cells in red. Scale bars: 200 μm. Statistical analysis was performed using the Kruskal-Wallis test, followed by Dunn's post-hoc test for multiple comparisons against day 0 (for metabolic activity) or day 1 (for viability). Statistical significance: *$P < 0.05$; **$P < 0.01$. (For interpretation of the references to color in this figure legend, the reader is referred to the Web version of this article.)

experiment. Likewise, the dermal hydrogels increased their cell metabolic activity from day 14, maintaining this level until the end of the experiment. Both hydrogels were able to maintain cell viability levels above 97 % during the assay (Fig. 3B, D, and E), as evidenced by the images acquired at 1, 7, 14, and 21 days.

The BT Skin was prepared in a three-layered way with the hypodermal layer at the bottom, the dermal layer in the middle, and the epidermal layer on top (Fig. 1A), and partially dehydrated. Similarly to the hypodermal and dermal hydrogels, the BT Skin substitute showed cell viability rates between 90.9 and 98 %, with a rise in metabolic activity rate from day 5, which remained in a plateau stage until the end of the experiment (Fig. 4A and B). In some areas of the hydrogels, cells were able to adhere and grow in contact with the surrounding cells (Fig. 4C). Moreover, to observe the distribution of the three cell types within each layer, hMSCs, hDFs, and hEKs were stained with Cell-Tracker™ Green CMFDA, CellTracker™ Red CMTPX, and CellTracker™ Green CMFDA, respectively. As can be observed in Fig. 4D, the three layers of the bioactive BT Skin hydrogel were well differentiated and maintained the structure throughout the study time.

To evaluate the interactions between hEKs, hDFs, and hMSCs within the BT Skin model, the secretion of growth factors into the conditioned medium at days 3 and 21 after biofabrication was analyzed. The results revealed active secretion across several growth factor families (Fig. S3). Overall, higher levels of growth factors were observed at day 3 compared to day 21. Among the angiogenic and vascular factors, VEGF and PDGF isoforms were notably abundant at both time points, with a general decrease by day 21, except for HGF, which increased its expression at day 21. Similarly, factors associated with ECM remodeling and proliferation, such as EGF and TGF-β isoforms, showed a decline over time, although bFGF levels were higher at day 21 than at day 3. Cell communication mediators, including IGF-I, IGF-II, and their binding proteins (IGFBPs), were consistently detected, with variations in their relative levels between the two time points. Neurotrophic and immunomodulatory factors, such as NT-3, NT-4, GM-CSF, and HGF, were present throughout the culture, with b-NGF exhibiting higher levels at day 21.
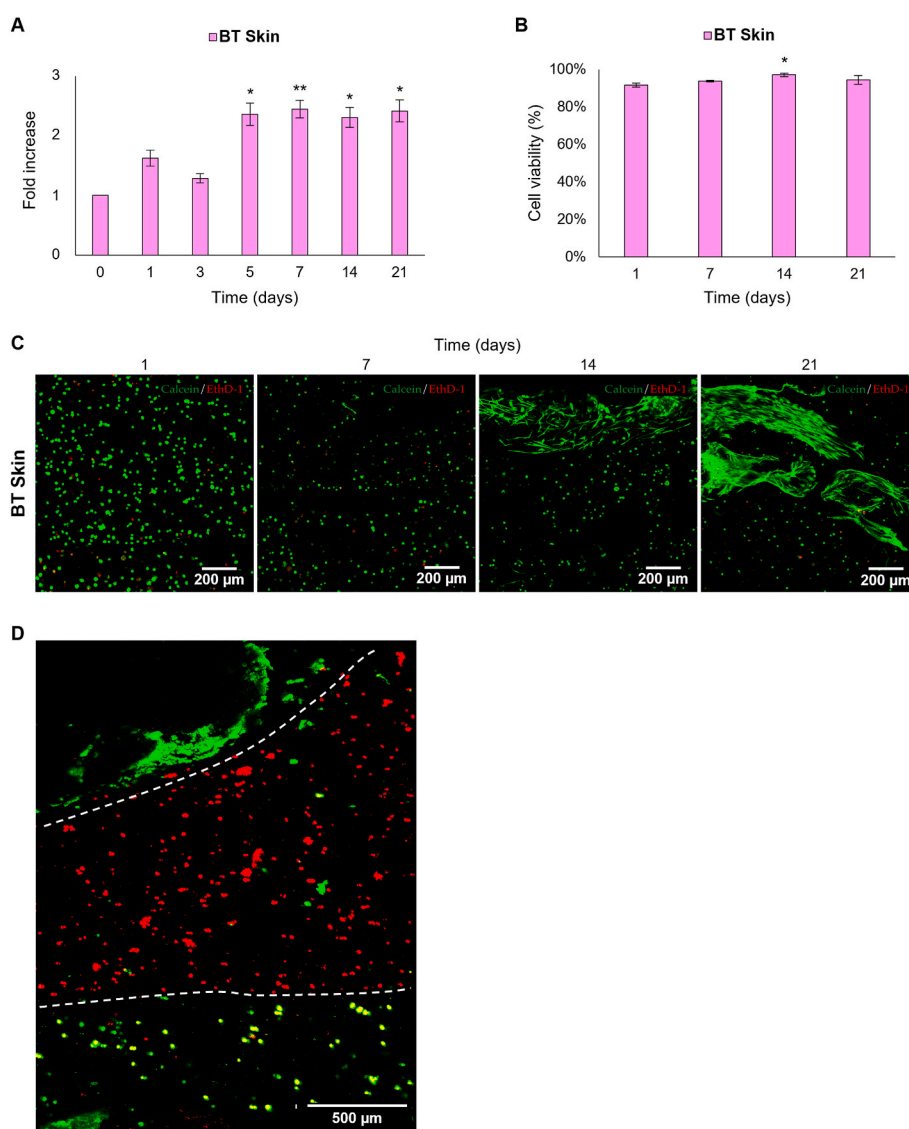

Fig. 4. BT Skin hydrogel (A) cell metabolic activity at 0, 1, 3, 5, 7, 14, and 21 days, and (B and C) viability at 1, 7, 14, and 21 days. (D) Confocal fluorescence image of BT Skin hydrogel after 21 days of culture: hEKs labeled in green on top, hDFs labeled in red in the middle, and hMSCs labeled in green at the bottom. Statistical analysis was performed using the Kruskal-Wallis test, followed by Dunn's post-hoc test for multiple comparisons against day 0 (for metabolic activity) or day 1 (for viability). Statistical significance compared to day 0: *P < 0.05; **P < 0.01. (For interpretation of the references to color in this figure legend, the reader is referred to the Web version of this article.)

3.4. In vivo assay

3.4.1. Wound healing assessment

Adequate wound stabilization was observed for all groups of mice after 4 weeks, with no complications (Fig. 5A), as seen in the POSAS assessment (Table S3). Wound closure was achieved in all groups after 4 weeks, although wound repair appeared to be faster in the Autograft, Cell-free BT Skin, and BT Skin groups than in the Control group. Similarly, wound resolution seemed more effective in the groups treated with Autograft and the BT Skin, followed by the Cell-free BT Skin group,

while the Control group experienced slower improvement (Fig. 5A).

Results evaluation by visual observation (Fig. 5A) correlated with quantitative analysis of wound/scar area (Fig. 5B), where significant differences were found between the Cell-free BT Skin and BT Skin groups when compared with the Control group at week 2, indicating a faster wound closure in these groups at this time. Additionally, the progression of each group relative to its week 2 measurements was also assessed, and all groups had significant differences in their wound/scar area at week 4 compared to their area at week 2. However, at week 6, only the Autograft group had significant differences compared to its week 2; and at
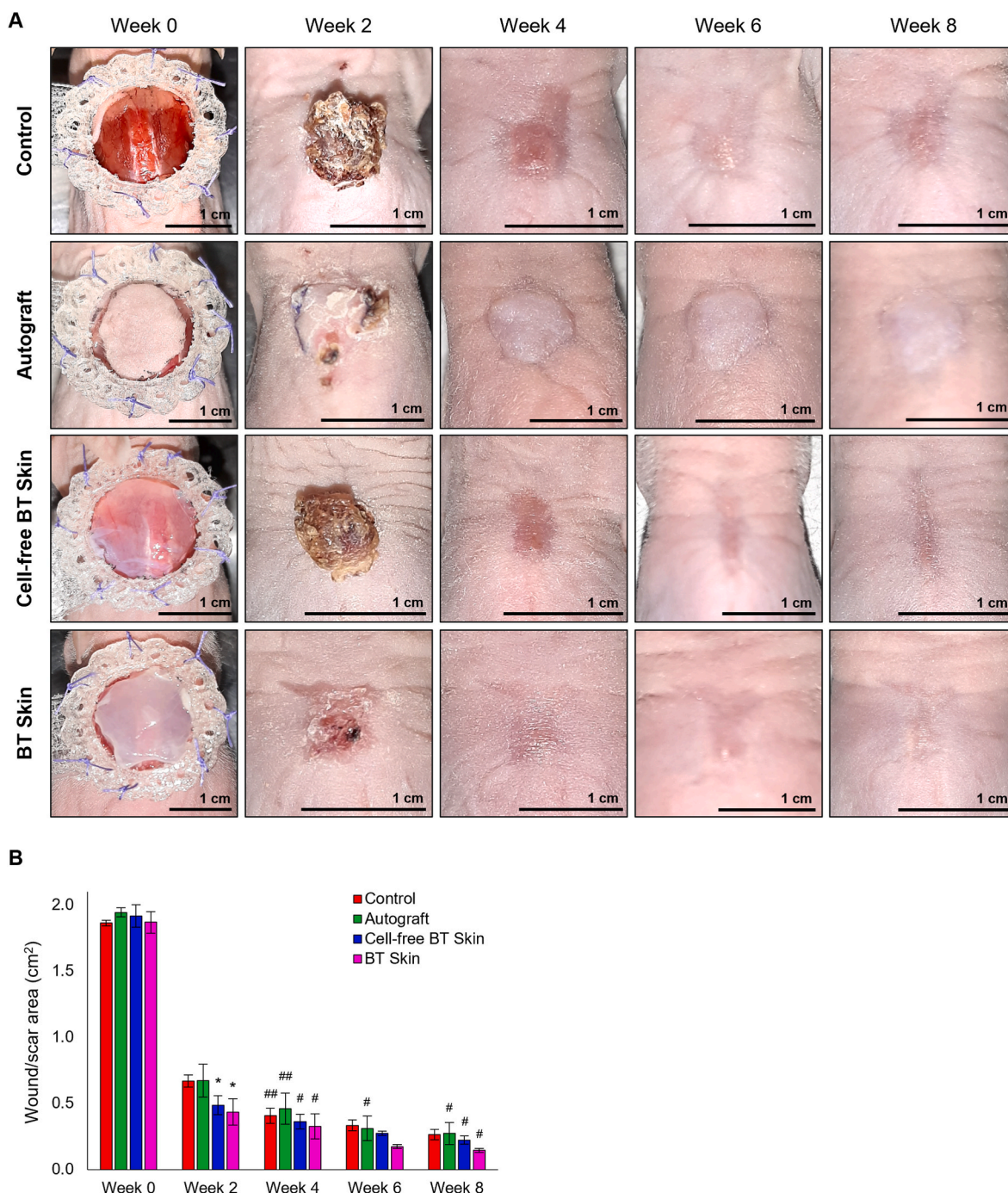

Fig. 5. (A) Macroscopic images of wound healing process over time. Type of treatment is indicated in each row, while progression time (week 0, 2, 4, 6, or 8) is represented in each column. Scale bars: 1 cm. (B) Quantitative evaluation of wound/scar area through time for all groups. Statistical analysis was performed using a mixed-effects model with the Geisser-Greenhouse correction, followed by Dunnett's post-hoc test for multiple comparisons, against the control group (for each week), and against week 2 (within each group). Statistical significance compared to control: *$P < 0.05$. Statistical significance compared to week 2: #$P < 0.05$; ##$P < 0.01$.

week 8, Autograft, Cell-free BT Skin, and BT Skin groups presented significant differences compared to their areas at week 2, indicating that the Control group experienced a slower reduction of the wound/scar area.

3.4.2. Homeostasis study

Temperature, pH, TEWL, elasticity, moisture, erythema, and pigmentation were monitored (Fig. 6 and Fig. S4), comparing all groups to the native skin of mice. Temperature (Fig. 6A, H, O, and V) and pH results (Fig. 6B, I, P, and W) showed a homogeneous evolution in all groups during the study, with almost no differences compared to native skin. Temperature values of all groups during the study ranged from 31.8 °C – 36.6 °C, overlapping the range of the native skin temperature (34.0 °C – 36.0 °C). Similarly, pH ranges of all groups (5.2–7.8) and native skin (6.4–7.3) also overlapped during the duration of the experiment. TEWL (Fig. 6C, J, Q, and X) showed significant differences between Control and Autograft groups compared to native skin at week 2, although there was an important decrease after 2 weeks in all groups, reaching native skin levels. Regarding elasticity (Fig. 6D, K, R, and Y), although Control, Cell-free BT Skin, and BT Skin groups showed an oscillatory behavior throughout the experiment, there were no significant differences between all groups and the native skin at the end of the experiment. Moisture monitorization (Fig. 6E, L, S, and Z) showed a similar tendency as TEWL. At week 2, the Control and Autograft groups displayed more statistically significant differences compared to native skin, whereas Cell-free BT Skin and BT Skin groups showed less pronounced differences, indicating a potentially milder deviation in moisture levels during the early stages of the experiment. However, there was a recovery after 2 weeks in all groups, restoring the native skin levels at 4 weeks.

Erythema assessment (Fig. 6F, M, T, and AA) of Cell-free BT Skin and BT Skin groups reported significantly higher levels than native skin at week 2, which were not significantly different after 4 weeks. Regarding pigmentation (Fig. 6G, N, U, and AB), Control and Autograft groups had more statistically significant differences compared to native skin at week 2, while Cell-free BT Skin and BT Skin had milder differences. All groups were able to reach native skin's melanin levels at the end of the experiment.

3.4.3. Histological and immunofluorescence analysis

H&E and Masson's Trichrome staining of wound biopsies (Fig. 7 and Fig. S5) showed a correct regeneration after 4 and 8 weeks in all groups; however, autograft, Cell-free BT Skin, and BT Skin groups presented a more complex dermal matrix structure closer to native skin than the control group, which showed a less dense dermal matrix structure 4 weeks after the surgical procedure. As can be observed in Fig. 8A, the immunofluorescence analysis showed an increased expression of fibronectin, a typical protein found in dermal ECM. Also, the expression of cytokeratin, a specific epidermal differentiation marker, was observed in all groups, showing that good re-epithelialization and epidermal differentiation were achieved.

Although a clearly distinguishable hypodermis with mature adipocytes was not yet observed in the regenerated tissue after 8 weeks, PPARγ, a key regulator of adipogenesis, was expressed in cells along the regenerated skin of the BT Skin group. Moreover, the expression of human HLA-A,B,C in the BT Skin group evidenced the persistence of human cells in the regenerated tissue. To further confirm this, an isotype control staining was performed, showing no detectable signal, which supports the specificity of the HLA-A,B,C staining and rules out nonspecific labeling (image not shown). Strong staining for mouse MHC class I (H-2K^d) was also observed, indicating significant host cell integration within the regenerated skin. Finally, VEGFA, CD31, and VE-Cadherin staining revealed the formation of new vascularization, with some vessel-like structures becoming apparent (Fig. 8B).

3.4.4. Inflammation assessment

The inflammatory profile associated with the biomaterials of the BT Skin was analyzed with a cytokine dot blot array (Fig. 9). Control mice showed a broader expression of diverse cytokines, while the cytokine profile of the Cell-free BT Skin mice appeared more specific and controlled. Both groups showed a relatively similar expression of several cytokines, with certain proinflammatory cytokines (such as IL-1β, IL-17A, IFN-γ, and MIP-1γ) showing slight elevations in the Cell-free BT Skin group, although their levels were not excessively higher than the Control; while Control mice exhibited a more active expression of proinflammatory cytokines such as IL-1α, IL-12 p70, TNF RI, TNF RII, and LIX. Other proinflammatory cytokines such as IL-12 p40/p70, TNF-α, and MIP-1α, were only expressed in the Control group. Some regulatory cytokines, like IL-9, IL-10, IL-13, MCP-1, Fractalkine, Eotaxin-2, or CD30 Ligand, were only expressed in the Control. Others like IL-4, Fas Ligand, or Eotaxin-1 were expressed in both groups but appeared higher in the Control. In contrast, the Cell-free BT Skin mice demonstrated elevated levels of SDF-1 α and I-309. Finally, the Control group showed a broader expression of chemotactic cytokines, while BLC and GM-CSF were similarly expressed in both groups, and RANTES was only expressed in Cell-free BT Skin.

4. Discussion

While the available variety of skin substitutes found in the market focuses on restoring the dermal and epidermal structures, the subcutaneous layer is often neglected. However, the hypodermis contributes to the epidermal differentiation process and provides mechanical and thermoregulatory properties to normal skin [19]. To answer this pitfall, three-layered skin substitutes that intend to better mimic the anatomy of the skin (epidermis, dermis, and hypodermis) have recently attracted attention. However, many "three-layered" skin substitutes or hydrogels actually consist of only two material layers, with hEKs seeded on top of the second layer being counted as the "third" layer [19,21,56]. In contrast, our BT Skin genuinely comprises three distinct biomaterial layers, with the third layer containing keratin and sphingolipids to resemble the key features of the native epidermis and provide a more suitable 3D environment for keratinocytes. In fact, due to the biological function, structural support, excellent biocompatibility, and favorable biodegradability characteristics of keratin, several previous studies have used it to create novel wound dressings that enhance the healing process, especially in chronic non-healing wounds [57–60]. Although the use of biomaterials like collagen, HA, gelatin, or fibrinogen is usual in the recent literature for the creation of three-layered skin substitutes [22,23], most of these three-layered constructs only use a one-component hydrogel, such as collagen I [21,61], or fibrin [20]. Here, we present a study in which the ECM of each one of the three layers of the skin has been customized to biofabricate a more bioactive and biologically-inspired skin substitute. The supplementation of the hydrogels with specific components of each skin layer, such as keratin, sphingolipids, dermatan sulfate, HA, or elastin, provides the BT Skin with an enhanced ECM complexity compared to its published counterparts, adding a plus to this bioactive and biomimetic skin substitute.

First, a physicochemical characterization was carried out for each of the three hydrogels and the BT Skin. The gelling time of the hydrogels is a relevant parameter during the biofabrication process. All three hydrogels showed manageable gelling times to work with, since acceptable 3D structures can be achieved with gelling times inferior to 15 min [62]. Another important factor is the viscosity of the hydrogel solutions, as higher viscosities tend to improve the 3D structure fidelity, but also negatively affect cell viability due to increased shear stresses [63]. The Agarose and Collagen I solutions, and the Neutralized Collagen I + Agarose blend demonstrated a Newtonian behavior, while Neutralized Collagen I showed a shear-thinning behavior. Moreover, Neutralized Collagen I exhibited a yield stress, manifested by a stress plateau at low shear rates, which is crucial for the shape retention of the
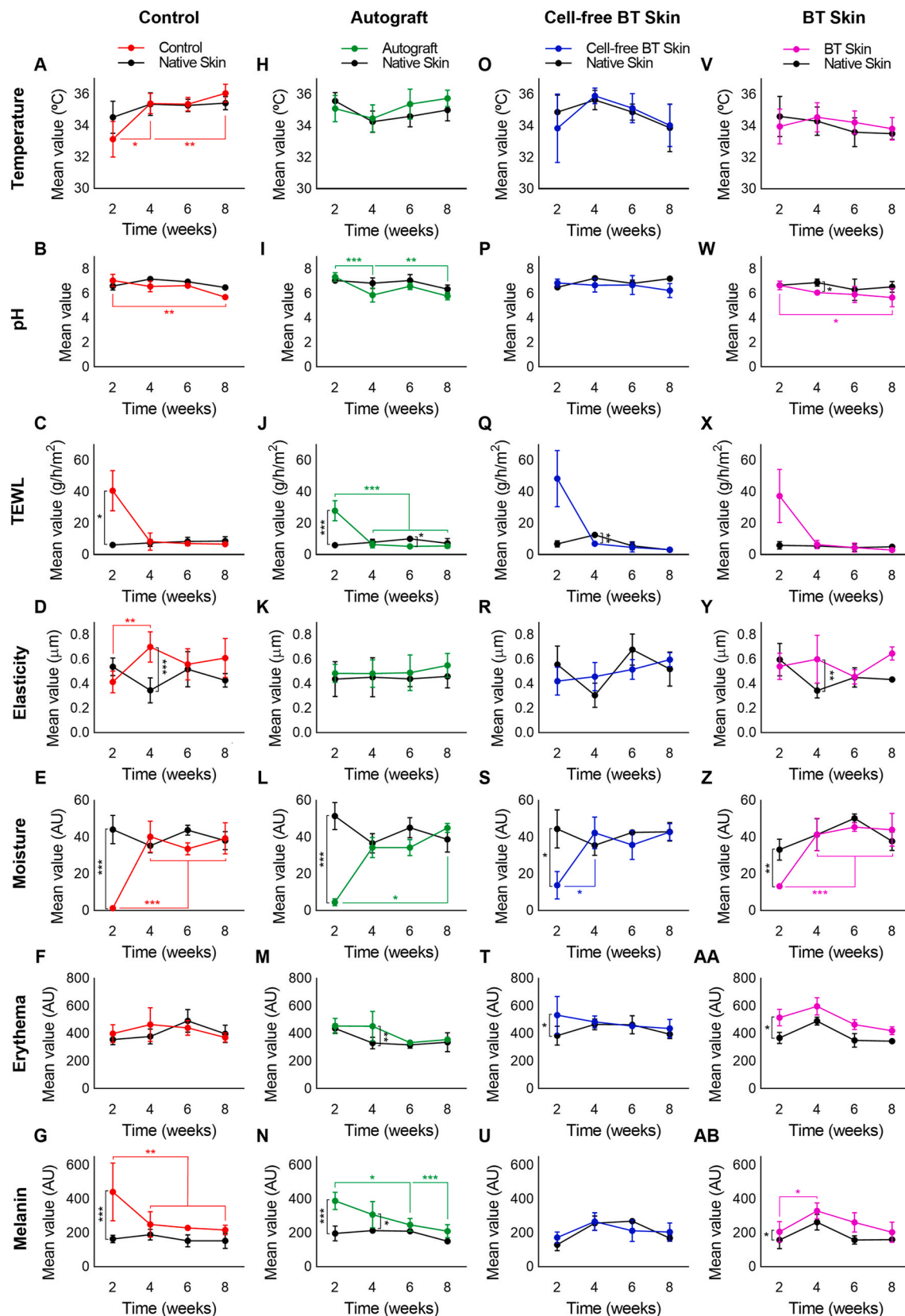
Fig. 6. Analysis of homeostasis parameters per week and group. Graphics show results for each group of treatment against the Native Skin group: (A–G) Control group, (H–N) Autograft group, (O–U) Cell-free BT Skin, and (V – AB) BT Skin. Results per week were calculated as the mean value of all mice measured at each time of study: Native Skin, Control, Autograft, Cell-free BT Skin, and BT Skin groups (n week 2, 4, 6, 8 = 8, 8, 4, 4). Statistical analysis was performed using one-way ANOVA, Welch ANOVA, or Kruskal-Wallis, as appropriate, followed by Tukey, Tamhane T2, or Dunn's post-hoc tests, respectively, for multiple comparisons. Statistical significance: *P < 0.05; **P < 0.01; ***P < 0.005.
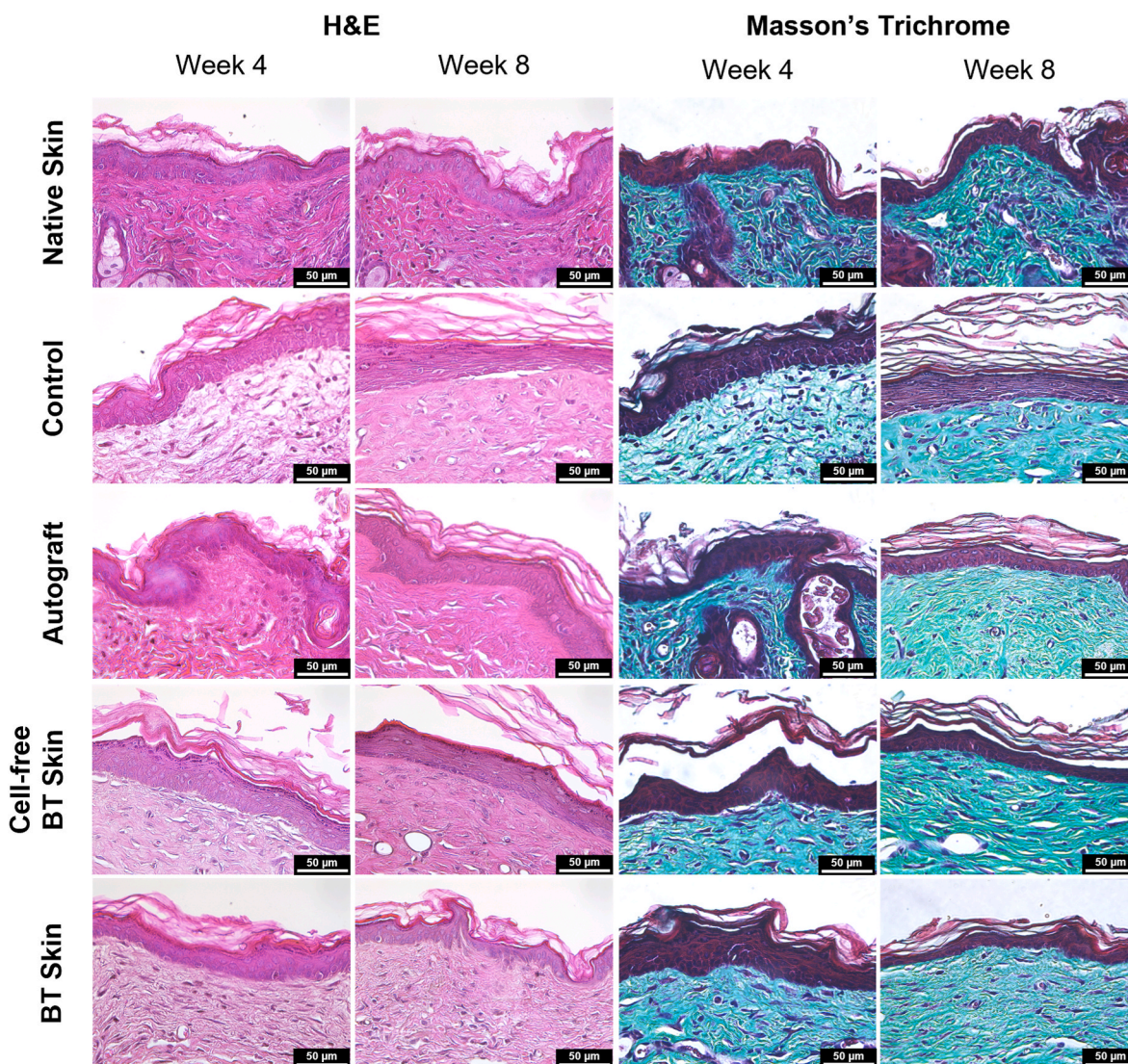
Fig. 7. H&E and Masson's Trichrome histological staining of biopsies of mice wound/scar area in Control, Autograft, Cell-free BT Skin, and BT Skin groups, and native skin after 4 and 8 weeks. Scale bars: 50 μm.

biofabricated construct [63].

The BT Skin showed a neutral pH (7.5 ± 0.1), suitable for skin TE, as it has been observed that collagen-based hydrogels should be pH-neutral to contribute to an optimal skin barrier function [64]. The hydrogel swelling is involved in nutrient and water transport within the surrounding media, providing remarkable mechanical resiliency [65], lowering the interfacial tension, promoting metabolite exchange, and improving cell viability [66]. The BT Skin presented a high swelling capacity that stabilized after 3 weeks and showed slow degradation rates, which could be useful in biofabrication applications that require volumetric accuracy and shape fidelity [67].

Fitting the mechanical characteristics of the targeted tissue is a relevant issue to help promote correct tissue regeneration [68]. Since the core blend of the hydrogels is agarose/collagen I-based, the biological advantages of the dermatan sulfate/HA, dermatan sulfate/HA/elastin, and keratin/sphingolipids supplementation could be combined with the agarose/collagen I compression modulus kPa range, which complies with native skin compression modulus. Both the hydrogels and the native skin measured in this study exhibited compression modulus results around the 10 kPa range, consistent with other values reported in the literature [69–71], further validating their suitability for mimicking the targeted tissue. Additionally, the BT Skin storage viscoelastic

modulus showed proper values close to those found in native skin. The biological performance of the hypodermal and dermal hydrogels, as well as the BT Skin hydrogel, revealed that both were able to maintain cell metabolic activity with high viability levels for 21 days. Additionally, the BT Skin was able to maintain its integrity after suffering a partial dehydration process, decreasing its thickness, and displaying the three differentiated cellular layers along its height for 21 days. This partial dehydration was used as a plastic compression technique [48], which rapidly removes the fluid excess of the supersaturated hydrogels, to produce mechanically strengthened hydrogels with a dense matrix and cellular structure. One of the main advantages of this technique used in the clinical field [43,47,72] is the ability to introduce microlayering, mechanical properties, and micrometric topographies that increase the biomimetic potential in minutes instead of days or weeks [48].

The analysis of growth factor secretion from the BT Skin provided insights into intercellular communication and coordination among hEKs, hDFs, and hMSCs across its three layers. Growth factor levels were generally higher at day 3 compared to day 21, likely due to the initial adaptation phase as cells transitioned from 2D monolayer cultures to the 3D hydrogel environment. This early phase likely triggered the secretion of factors to support ECM remodeling and stabilization. Additionally, the elevated EGF levels at day 3 can be attributed to the use of
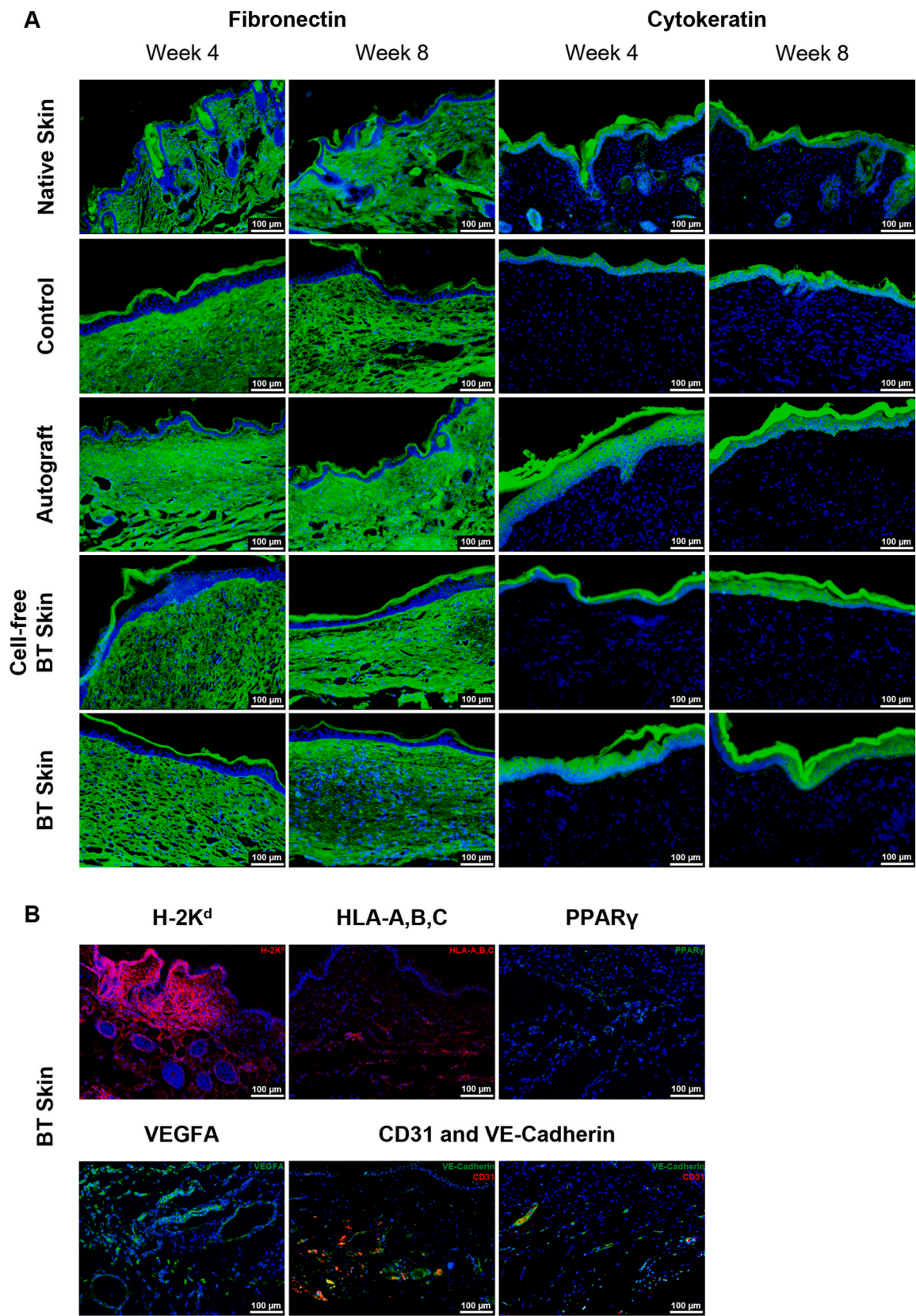
Fig. 8. Fluorescence microscopy observations of (A) fibronectin and cytokeratin profiles of mice wound/scar area in Control, Autograft, Cell-free BT Skin, and BT Skin groups, and native skin biopsies after 4 and 8 weeks; and (B) mouse H-2K^d (MHC class I), human HLA-A,B,C, PPARγ, VEGFA, CD31, and VE-Cadherin profiles in the BT Skin group after 8 weeks. Fibronectin, cytokeratin, PPARγ, VEGFA, and VE-Cadherin are stained in green, while H-2K^d, HLA-A,B,C, and CD31 are stained in red, and nuclei are shown in blue. Scale bars: 100 μm. (For interpretation of the references to color in this figure legend, the reader is referred to the Web version of this article.)
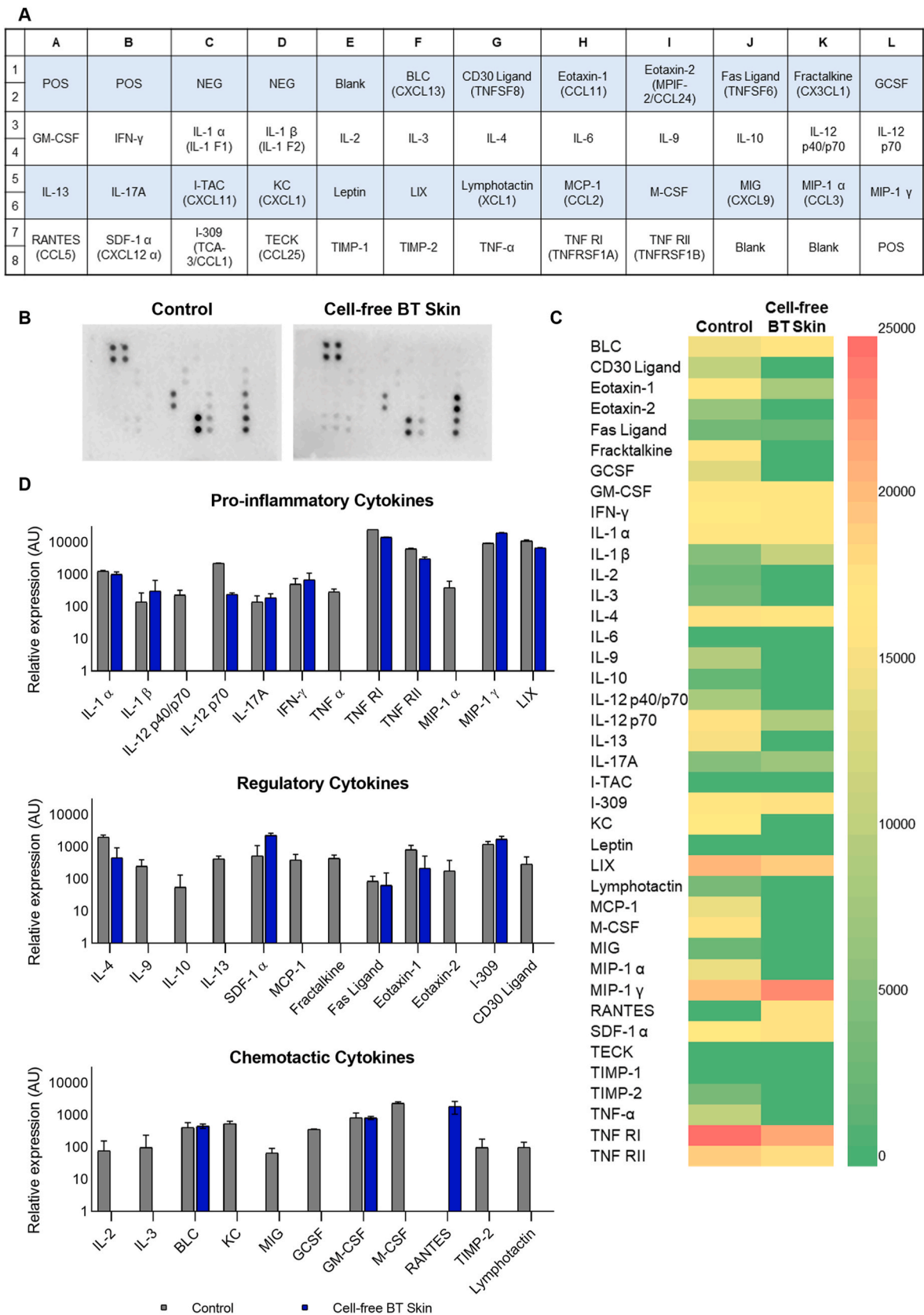
Fig. 9. _In vivo_ inflammation assay. (A) Cytokine antibody array map. (B) Revealed cytokine antibody dot blot array membranes for Control and Cell-free BT Skin. (C) Heat map of the relative expression of cytokines in Control and Cell-free BT Skin groups, as determined by the dot blot array assay. (D) Quantification of the relative expression of cytokines in Control and Cell-free BT Skin groups, classified as pro-inflammatory, regulatory, and chemotactic cytokines.

keratinocyte medium, supplemented with EGF, during the initial culture phase. Over time, growth factor secretion decreased, paralleling the stabilization of cellular metabolic activity observed after approximately a week. However, the sustained release of various factors at day 21 underscores ongoing intercellular communication and dynamic activity within the BT Skin. Angiogenic factors, such as VEGF and PDGF isoforms, secreted by hMSCs and hDFs, likely support nutrient exchange and hEKs proliferation [73,74]. ECM remodeling and proliferative factors, including EGF, FGFs, and TGF-β isoforms, promote ECM organization and epithelial regeneration [75–77]. Notably, the higher bFGF levels at day 21 suggest ongoing fibroblast activity and remodeling. Factors mediating cell communication, such as IGFs and their binding proteins (IGFBPs), regulate growth, survival, and differentiation [78–80]. Neurotrophic and immunomodulatory factors (e.g., b-NGF, NT-3, NT-4, GM-CSF, and M-CSF) enhance skin innervation and modulate immune responses to support homeostasis, respectively [81,82]. Interestingly, some neurotrophic factors also exhibit functions beyond their classical roles in the nervous system. For example, NGF and NT factors are secreted by different skin cell types such as keratinocytes or fibroblasts, and promote their proliferation, migration, and differentiation [83,84]. Furthermore, the increased levels of HGF, b-NGF, and bFGF at day 21 may indicate a shift toward a more stable and regulated remodeling phase. In conclusion, the BT Skin model demonstrates active and sustained intercellular communication, reflecting its potential for coordinated skin regeneration processes.

Wound healing is a complex biological process that leads to resolution (regeneration) or repair (healing) [85]. The tissue regenerates the ECM, cell population, and function in wound resolution, while scarring or fibrosis due to the lack of ability to fully regenerate a tissue occurs in wound repair [86]. In the current study, we evaluated the closure rate and homeostatic and histological characteristics of excision skin wound mice models treated with BT Skin, Cell-free BT Skin, and Autograft, compared to an untreated control. Cell-free BT Skin and BT Skin showed a higher reduction of the wound/scar area than the control after 2 weeks, as well as similar results to Autograft in the POSAS scale. With the BT Skin substitute, we reached an early wound closure after 14 days, while other collagen-based three-layered constructs seen in the literature did not achieve wound closure after that time [21], or even after 21 days [87]. Early wound closure is important to avoid a late re-epithelialization, reduce the risk of infections, prevent complications, and facilitate improved cosmetic outcomes and minimal scarring [7].

Among the components of the ECM, collagen, HA, GAGs, and elastin are known to improve wound healing [88]. *In vivo* studies have demonstrated that collagen hydrogels are effective wound healing agents by enhancing ECM remodeling and accelerating tissue repair [26]. HA, actively secreted by fibroblasts at the wound sites, is a key component of early granulation tissue. It supports scarless healing by inhibiting platelet degranulation, reducing inflammation, and preventing excessive collagen deposition. Moreover, HA facilitates the migration of keratinocytes to the wound site, promoting re-epithelialization and contributing to the wound healing process [89,90]. Although elastin typically appears in later wound healing phases, it is conventionally recognized for its structural role in providing ECM elasticity. Additionally, elastic fibers in the dermis influence cell phenotypes and regulate matrix and cytokine production, crucial for skin homeostasis and repair [91]. Moreover, elastin-based scaffolds have been shown to support cell growth and accelerate wound closure [92,93]. These include scaffolds derived from ECM-based elastin, the elastin precursor tropoelastin, and acellular dermal matrices [94–98].

In addition, it has been shown that hydrogels loaded with cells or cytokines enhance cell proliferation, promote vascularization and re-epithelialization, and reduce wound healing time [26]. Cells including keratinocytes, fibroblasts, endothelial cells, and macrophages, interact to facilitate wound healing. For example, keratinocytes and fibroblasts engage in a double paracrine interaction, where keratinocytes stimulate fibroblasts to produce growth factors that subsequently stimulate keratinocyte proliferation [99]. Additionally, they play a crucial role in communicating with other cell types, such as immune cells, to support tissue repair and homeostasis [91]. During wound healing, MSCs from the subcutaneous fat regulate early and mid-phase inflammation and support dermal tissue restoration. MSCs secrete various bioactive compounds, including growth factors such as VEGF, keratinocyte growth factor, and fibroblast growth factor 2, which are critical for wound healing as they stimulate angiogenesis, enhance skin cell proliferation, and promote ECM formation [77,100]. Altogether, these factors may explain why the BT Skin and Cell-free BT Skin groups showed significant differences compared to the Control group at two weeks.

Regarding homeostasis and epidermal barrier function, autograft, Cell-free BT Skin, and BT Skin showed similar results to native skin. The lack of significant differences in skin temperature between the groups indicates the correct restoration of this function. When skin is harmed, its barrier function is compromised resulting in a high water loss [101, 102] and, consequently, a reduction of skin moisture [103,104]. All groups were able to restore the skin barrier integrity, showing similar TEWL and moisture values to native skin by the end of the experiment. However, BT Skin and Cell-free BT Skin showed less pronounced differences compared to native skin at week 2, which could help preserve the wound microenvironment during this early phase, potentially supporting the healing process.

The redness of the skin caused by hyperemia in superficial blood vessels can be studied by analyzing the erythema. Control and Autograft presented similar levels to native skin at week 2, while the Cell-free BT Skin and BT Skin showed significantly higher values at week 2. These higher levels could be a result of angiogenesis caused by the hydrogel's wound healing properties [38,41,105–107].

Melanin is a pigment produced by melanocytes whose main role is to minimize the deleterious effects of UVR [108]. Within a wound, melanocytes would be expected to be the first cells to repopulate the damaged area, as part of the initial wound healing response. However, melanocytes seem to enter the wound later once it has re-epithelialized [109]. In the present study, both Cell-free BT Skin and BT Skin groups had already recovered native skin melanin levels at week 2, while Control and Autograft groups were not able to reach those values until at least week 4. The outcome of this last condition was expected since skin autografts can experience an abrupt reduction of the graft's melanocyte population when transplanted, which gradually increases between 1 and 3 weeks after transplantation [110].

In addition, histological and immunofluorescence staining revealed that newly-formed healed skin showed a structure and morphology relatively similar to native skin after 4 and 8 weeks, presenting a multi-layered epithelium, with a structured dermis and fibroblasts layout, although an absence of skin appendages and rete ridges was observed. Nevertheless, unlike the Control group, which showed a less dense dermal matrix [111], Autograft, Cell-free BT Skin, and BT Skin groups developed a seemingly more reliable dermal matrix that resembled native skin. Also, fibronectin and cytokeratin, which are involved in epidermal stability and re-epithelization, were abundantly expressed in healed skin, demonstrating the reconstruction and remodeling of the wounds [112,113]. The regenerated tissue sections did not display a clearly distinguishable hypodermis, possibly due to adipogenesis requiring a prolonged timeframe to achieve complete hMSC differentiation into preadipocytes and their subsequent maturation into adipocytes [114]. Moreover, this process relies on vascularization, angiogenic support, and signaling pathways, and it is linked to hair follicle cycling [114–117], which may not have fully developed yet within the 8-week duration of the study. Nevertheless, the expression of PPARγ, a transcription factor critical for initiating adipogenic pathways [115], was observed in cells distributed throughout the regenerated skin of the BT Skin group, suggesting that some cells may have entered the early stages of adipogenic differentiation. The staining of VEGFA, a pro-angiogenic factor essential for stimulating endothelial cell proliferation and new blood vessel formation; CD31, an endothelial cell marker commonly

used to identify blood vessels and evaluate angiogenesis; and VE-Cadherin, an endothelial-specific adhesion molecule that plays a crucial role in maintaining vascular integrity and regulating endothelial cell-cell junctions, indicated the formation of new vascular structures, with some vessel-like formations becoming visible in the tissue, in concordance with the high erythema levels observed, likely due to stimulation of vascularization and angiogenesis by some components of the BT Skin, such as HA and dermatan sulfate [39,118–120]. Finally, the persistence of the BT Skin's human cells in the regenerated skin was confirmed by the expression of human HLA, underscoring their contribution to the healing process.

Understanding the potential immune responses elicited by skin substitutes is crucial for ensuring their safety and therapeutic efficacy. In this study, cytokine profiling on immunocompetent mice revealed that the biomaterials of the BT Skin did not exacerbate the systemic inflammatory response beyond what was induced by the wound produced to implant the hydrogel subcutaneously. Control mice expressed more diverse cytokines, while the Cell-free BT Skin group demonstrated a more regulated cytokine profile, with modest elevations in proinflammatory markers such as IL-1β, IL-17A, and IFN-γ, alongside increased levels of SDF-1α, associated with progenitor cell recruitment and tissue repair [121], and RANTES, whose presence during wound healing may indirectly contribute to the repair process by the recruitment of reparative cells and the regulation of the inflammatory environment [122,123]. In contrast, the control group exhibited a broader expression of cytokines, including TNF-α, TNF RI, MIP-1α, and LIX, which are linked to acute and chronic inflammation, as well as a more diverse variety of chemotactic cytokines like MIG, reflecting a more generalized and less regulated immune activation. These findings suggest that the materials of the BT Skin promote a balanced inflammatory environment that may support regeneration while minimizing excessive immune activation. The presence of immunomodulatory components like HA or collagen, which have been widely reported to have anti-inflammatory and immunomodulatory effects [106,124–126], likely contributes to the regulation of this controlled response, highlighting the potential of BT Skin as a safe and effective therapeutic alternative for skin regeneration.

In summary, these results support that the combination of human cells with the biomaterials forming the BT Skin promoted skin wound healing and regeneration processes. BT Skin could be a promising alternative to autografts for skin wound treatment in the near future. We aimed to prioritize faster treatment options, recognizing the importance of rapid intervention in wound management, and developing a substitute that could be applied as quickly as possible. Additionally, the BT Skin preparation process required one week of culture to ensure adequate cell attachment and integration into the hydrogel matrix, making it ready for implantation without complete tissue maturation. This approach aligns with other studies reporting similar preparation timelines [43], though some strategies in the literature require longer periods (e.g. 12–41 days [127–129]) to achieve more mature constructs. On the other hand, the Cell-free BT Skin, which also demonstrated adequate performance, offers the benefit of same-day preparation and application, and adds flexibility in scenarios where cell availability or time constraints are critical, as it could be used as a medical device.

Overall, these results indicate that BT Skin could represent a potential alternative to autografts for clinical applications, particularly in cases where donor sites are unavailable or contraindicated, although further long-term preclinical and clinical studies are necessary to determine the potential usefulness of this skin substitute.

5. Conclusions

We present a bioactive BT Skin that shows epidermal, dermal, and hypodermal layers based on skin-derived biomaterials (collagen I, dermatan sulfate, HA, elastin, keratin, and sphingolipids) and a tissue-specific cell type distribution. The skin substitute can help to restore the physiological homeostatic equilibrium and epidermal barrier function of skin wounds. The BT Skin promotes wound healing and regeneration of healthy skin with a histological architecture that resembles natural skin with a similar expression of cytokeratin and fibronectin, which participate in epidermal stability and re-epithelization. Moreover, the biomaterials of the BT Skin demonstrated excellent biocompatibility and a controlled inflammatory environment that supports regeneration while minimizing excessive immune activation. In addition, the hydrogels used to create the BT Skin showed desirable physicochemical and rheological properties, as well as optimal biological properties, demonstrating intercellular communication through the release of growth factors. These results highlight the BT Skin as a promising alternative to autografts, offering comparable results while avoiding their inherent drawbacks. Moreover, the Cell-free BT Skin also demonstrated strong potential, enabling same-day application and clinical translation as a medical device. These findings suggest that the BT Skin is a promising hydrogel formulation with high potential for clinical application in skin TE.

CRediT authorship contribution statement

Carlos Chocarro-Wrona: Writing – review & editing, Writing – original draft, Visualization, Methodology, Investigation, Formal analysis, Data curation, Conceptualization. **Paula Pleguezuelos-Beltrán:** Writing – review & editing, Visualization, Methodology, Investigation, Formal analysis, Data curation. **Julia López de Andrés:** Investigation. **Cristina Antich:** Investigation. **Juan de Vicente:** Resources, Methodology, Funding acquisition. **Gema Jiménez:** Funding acquisition. **Salvador Arias-Santiago:** Resources, Methodology. **Patricia Gálvez-Martín:** Writing – review & editing, Supervision, Resources, Project administration, Funding acquisition. **Elena López-Ruiz:** Writing – review & editing, Supervision, Resources, Project administration, Funding acquisition, Conceptualization. **Juan Antonio Marchal:** Writing – review & editing, Supervision, Resources, Project administration, Funding acquisition, Conceptualization.

Ethics approval and consent to participate

All human samples used in this study were obtained after informed consent and authorization was provided from the Granada Provincial Ethics Committee (Ministry of Health and Families, Andalusia, Spain, reference: 0467-N-20).

All animal handling procedures followed the national and European Union legislation (Spanish RD 53/2013 and EU Directive 2010/63) for the protection of animals used for scientific purposes and following the Ethical Principles and Guidelines for the Use of Animals approved by Provincial Ethics Committees of Granada (reference number: June 1, 2022/081).

Availability of data and materials

All data generated or analyzed during this study are included in this published article and its supplementary information files.

Funding

Declaration of competing interest

The authors declare the following financial interests/personal relationships which may be considered as potential competing interests: Patricia Galvez-Martin reports a relationship with Bioibérica SA that includes: employment. If there are other authors, they declare that they have no known competing financial interests or personal relationships that could have appeared to influence the work reported in this paper.

Acknowledgments

Appendix A. Supplementary data

Supplementary data to this article can be found online at https://doi.org/10.1016/j.mtbio.2025.101592.

Data availability

Data will be made available on request.

References

[1] R.D. Sontheimer, Skin is not the largest organ, J. Invest. Dermatol. 134 (2014) 581–582, https://doi.org/10.1038/jid.2013.335.

[2] A. Baroni, E. Buommino, V. De Gregorio, E. Ruocco, V. Ruocco, R. Wolf, Structure and function of the epidermis related to barrier properties, Clin. Dermatol. 30 (2012) 257–262, https://doi.org/10.1016/j.clindermatol.2011.08.007.

[3] M. Boer, E. Duchnik, R. Maleszka, M. Marchlewicz, Structural and biophysical characteristics of human skin in maintaining proper epidermal barrier function, Adv. Dermatol. Allergol. 1 (2016) 1–5, https://doi.org/10.5114/pdia.2015.48037.

[4] P. Pleguezuelos-Beltrán, S. Herráiz-Gil, D. Martínez-Moreno, I. Medraño-Fernandez, C. León, S. Guerrero-Aspizua, Regenerative cosmetics: skin tissue engineering for anti-aging, repair, and hair restoration, Cosmetics 11 (2024) 121, https://doi.org/10.3390/cosmetics11040121.

[5] C.M. Chuong, B.J. Nickoloff, P.M. Elias, L.A. Goldsmith, E. Macher, P. A. Maderson, J.P. Sundberg, H. Tagami, P.M. Plonka, K. Thestrup-Pedersen, B. A. Bernard, J.M. Schröder, P. Dotto, C.H. Chang, M.L. Williams, K.R. Feingold, L. E. King, A.M. Kligman, J.L. Rees, E. Christophers, What is the 'true' function of skin? Exp. Dermatol. 11 (2002) 159–187, https://doi.org/10.1034/j.1600-0625.2002.00112.x.

[6] C. Dai, S. Shih, A. Khachemoune, Skin substitutes for acute and chronic wound healing: an updated review, J. Dermatol. Treat. 31 (2020) 639–648, https://doi.org/10.1080/09546634.2018.1530443.

[7] P. Pleguezuelos-Beltrán, P. Gálvez-Martín, D. Nieto-García, J.A. Marchal, E. López-Ruiz, Advances in spray products for skin regeneration, Bioact. Mater. 16 (2022) 187–203, https://doi.org/10.1016/j.bioactmat.2022.02.023.

[8] C. Chocarro-Wrona, E. López-Ruiz, M. Perán, P. Gálvez-Martín, J.A. Marchal, Therapeutic strategies for skin regeneration based on biomedical substitutes, J. Eur. Acad. Dermatol. Venereol. 33 (2019) 484–496, https://doi.org/10.1111/jdv.15391.

[9] N.M. Vecin, R.S. Kirsner, Skin substitutes as treatment for chronic wounds: current and future directions, Front. Med. 10 (2023), https://doi.org/10.3389/fmed.2023.1154567.

[10] J. Kanitakis, Anatomy, histology and immunohistochemistry of normal human skin, Eur. J. Dermatol. 12 (2002) 390–399, quiz 400–399.

[11] K. Bocheńska, M. Gabig-Cimińska, Unbalanced sphingolipid metabolism and its implications for the pathogenesis of psoriasis, Molecules 25 (2020) 1130, https://doi.org/10.3390/molecules25051130.

[12] A. Shpichka, D. Butnaru, E.A. Bezrukov, R.B. Sukhanov, A. Atala, V. Burdukovskii, Y. Zhang, P. Timashev, Skin tissue regeneration for burn injury, Stem Cell Res. Ther. 10 (2019) 94, https://doi.org/10.1186/s13287-019-1203-3.

[13] M. Ríos-Galacho, D. Martínez-Moreno, E. López-Ruiz, P. Gálvez-Martín, J. A. Marchal, An overview on the manufacturing of functional and mature cellular skin substitutes, Tissue Eng Part B Rev 28 (2022) 1035–1052, https://doi.org/10.1089/ten.teb.2021.0131.

[14] H. Ying, J. Zhou, M. Wang, D. Su, Q. Ma, G. Lv, J. Chen, In situ formed collagen-hyaluronic acid hydrogel as biomimetic dressing for promoting spontaneous wound healing, Mater. Sci. Eng. C 101 (2019) 487–498, https://doi.org/10.1016/j.msec.2019.03.093.

[15] L. Kang, Y. Zhou, X. Chen, Z. Yue, X. Liu, C. Baker, G.G. Wallace, Fabrication and characterization of an electro-compacted collagen/elastin/hyaluronic acid sheet as a potential skin scaffold, Macromol. Biosci. 23 (2023), https://doi.org/10.1002/mabi.202300220.

[16] U. Anderegg, N. Halfter, M. Schnabelrauch, V. Hintze, Collagen/glycosaminoglycan-based matrices for controlling skin cell responses, Biol. Chem. 402 (2021) 1325–1335, https://doi.org/10.1515/hsz-2021-0176.

[17] M. Hosseini, A. Shafiee, Engineering bioactive scaffolds for skin regeneration, Small 17 (2021), https://doi.org/10.1002/smll.202101384.

[18] M. Stojic, J. Ródenas-Rochina, M.L. López-Donaire, I. González de Torre, M. González Pérez, J.C. Rodríguez-Cabello, L. Vojtová, J.L. Jorcano, D. Velasco, Elastin-plasma hybrid hydrogels for skin tissue engineering, Polymers 13 (2021) 2114, https://doi.org/10.3390/polym13132114.

[19] A. Monfort, M. Soriano-Navarro, J.M. García-Verdugo, A. Izeta, Production of human tissue-engineered skin trilayer on a plasma-based hypodermis, J Tissue Eng Regen Med 7 (2013) 479–490, https://doi.org/10.1002/term.546.

[20] M. Keck, A. Gugerell, J. Kober, Engineering a multilayered skin substitute with keratinocytes, fibroblasts, adipose-derived stem cells, and adipocytes, in: Methods in Molecular Biology, Humana Press Inc., 2019, pp. 149–157, https://doi.org/10.1007/978-1-4939-9473-1_12.

[21] J. Zimoch, D. Zielinska, K. Michalak-Micka, D. Rütsche, R. Böni, T. Biedermann, A.S. Klar, Bio-engineering a prevascularized human tri-layered skin substitute containing a hypodermis, Acta Biomater. 134 (2021) 215–227, https://doi.org/10.1016/j.actbio.2021.07.033.

[22] A.M. Jorgensen, A. Gorkun, N. Mahajan, K. Willson, C. Clouse, C.G. Jeong, M. Varkey, M. Wu, S.J. Walker, J.A. Molnar, S.V. Murphy, S.J. Lee, J.J. Yoo, S. Soker, A. Atala, Multicellular bioprinted skin facilitates human-like skin architecture in vivo, Sci. Transl. Med. 15 (2023), https://doi.org/10.1126/scitranslmed.adf7547.

[23] J. Jäger, I. Vahav, M. Thon, T. Waaijman, B. Spanhaak, M. de Kok, R.K. Bhogal, S. Gibbs, J.J. Koning, Reconstructed human skin with hypodermis shows essential role of adipose tissue in skin metabolism, Tissue Eng Regen Med (2024) 1–13, https://doi.org/10.1007/s13770-023-00621-1.

[24] T.M. Avelino, S.V. Harb, D. Adamoski, L.C.M. Oliveira, C.D.S. Horinouchi, R.J. de Azevedo, R.A. Azoubel, V.K. Thomaz, F.A.H. Batista, M.A. d'Ávila, P.L. Granja, A. C.M. Figueira, Unveiling the impact of hypodermis on gene expression for advancing bioprinted full-thickness 3D skin models, Commun. Biol. 7 (2024) 1437, https://doi.org/10.1038/s42003-024-07106-4.

[25] I.N. Amirrah, Y. Lokanathan, I. Zulkiflee, M.F.M.R. Wee, A. Motta, M.B. Fauzi, A comprehensive review on collagen type I development of biomaterials for tissue engineering: from biosynthesis to bioscaffold, Biomedicines 10 (2022) 2307, https://doi.org/10.3390/biomedicines10092307.

[26] Y. Zhang, Y. Wang, Y. Li, Y. Yang, M. Jin, X. Lin, Z. Zhuang, K. Guo, T. Zhang, W. Tan, Application of collagen-based hydrogel in skin wound healing, Gels 9 (2023) 185, https://doi.org/10.3390/gels9030185.

[27] J. Killat, K. Reimers, C. Choi, S. Jahn, P. Vogt, C. Radtke, Cultivation of keratinocytes and fibroblasts in a three-dimensional bovine collagen-elastin matrix (Matriderm®) and application for full thickness wound coverage in vivo, Int. J. Mol. Sci. 14 (2013) 14460–14474, https://doi.org/10.3390/ijms140714460.

[28] B. Ledford, C. Barron, M. Van Dyke, J.-Q. He, Keratose hydrogel for tissue regeneration and drug delivery, Semin. Cell Dev. Biol. 128 (2022) 145–153, https://doi.org/10.1016/j.semcdb.2021.06.017.

[29] P. Hill, H. Brantley, M. Van Dyke, Some properties of keratin biomaterials: kerateines, Biomaterials 31 (2010) 585–593, https://doi.org/10.1016/j.biomaterials.2009.09.076.

[30] W.M. Holleran, Y. Takagi, Y. Uchida, Epidermal sphingolipids: metabolism, function, and roles in skin disorders, FEBS Lett. 580 (2006) 5456–5466, https://doi.org/10.1016/j.febslet.2006.08.039.

[31] A.M. Ionescu, J. Chato-Astrain, J. de la C. Cardona, F. Campos, M.M. Pérez, M. Alaminos, I. Garzón, Evaluation of the optical and biomechanical properties of bioengineered human skin generated with fibrin-agarose biomaterials, J. Biomed. Opt. 25 (2020) 1, https://doi.org/10.1117/1.JBO.25.5.055002.

[32] E. Cambria, S. Brunner, S. Heusser, P. Fisch, W. Hitzl, S.J. Ferguson, K. Wuertz-Kozak, Cell-laden agarose-collagen composite hydrogels for mechanotransduction studies, Front. Bioeng. Biotechnol. 8 (2020), https://doi.org/10.3389/fbioe.2020.00346.

[33] R. Parenteau-Bareil, R. Gauvin, F. Berthod, Collagen-based biomaterials for tissue engineering applications, Materials 3 (2010) 1863–1887, https://doi.org/10.3390/ma3031863.

[34] S.F. Penc, B. Pomahac, T. Winkler, R.A. Dorschner, E. Eriksson, M. Herndon, R. L. Gallo, Dermatan sulfate released after injury is a potent promoter of fibroblast growth factor-2 function, J. Biol. Chem. 273 (1998) 28116–28121, https://doi.org/10.1074/jbc.273.43.28116.

[35] P.H.A. Lee, J.M. Trowbridge, K.R. Taylor, V.B. Morhenn, R.L. Gallo, Dermatan sulfate proteoglycan and glycosaminoglycan synthesis is induced in fibroblasts by transfer to a three-dimensional extracellular environment, J. Biol. Chem. 279 (2004) 48640–48646, https://doi.org/10.1074/jbc.M407241200.

[36] S. Mizumoto, S. Yamada, The specific role of dermatan sulfate as an instructive glycosaminoglycan in tissue development, Int. J. Mol. Sci. 23 (2022) 7485, https://doi.org/10.3390/ijms23137485.

[37] J.J. Greene, D.M. Sidle, The hyaluronic acid fillers: current understanding of the tissue device interface, Facial Plast Surg Clin North Am 23 (2015) 423–432, https://doi.org/10.1016/j.fsc.2015.07.002.

[38] M.N. Leite, M.A.C. Frade, Efficacy of 0.2% hyaluronic acid in the healing of skin abrasions in rats, Heliyon 7 (2021) e07572, https://doi.org/10.1016/j.heliyon.2021.e07572.

[39] E.L. Pardue, S. Ibrahim, A. Ramamurthi, Role of hyaluronan in angiogenesis and its utility to angiogenic tissue engineering, Organogenesis 4 (2008) 203–214, https://doi.org/10.4161/org.4.4.6926.

[40] B.M. Teh, Y. Shen, P.L. Friedland, M.D. Atlas, R.J. Marano, A review on the use of hyaluronic acid in tympanic membrane wound healing, Expert Opin Biol Ther 12 (2012) 23–36, https://doi.org/10.1517/14712598.2012.634792.

[41] A.M. Juncan, D.G. Moisă, A. Santini, C. Morgovan, L.-L. Rus, A.L. Vonica-Țincu, F. Loghin, Advantages of hyaluronic acid and its combination with other bioactive ingredients in cosmeceuticals, Molecules 26 (2021) 4429, https://doi.org/10.3390/molecules26154429.

[42] L.J. Pourchet, A. Thepot, M. Albouy, E.J. Courtial, A. Boher, L.J. Blum, C.A. Marquette, Human skin 3D bioprinting using scaffold-free approach, Adv Healthc Mater 6 (2017) 1601101, https://doi.org/10.1002/adhm.201601101.

[43] Á. Sierra-Sánchez, A. Fernández-González, A. Lizana-Moreno, O. Espinosa-Ibáñez, A. Martinez-Lopez, J. Guerrero-Calvo, N. Fernández-Porcel, A. Ruiz-García, A. Ordóñez-Luque, V. Carriel, S. Arias-Santiago, Hyaluronic acid biomaterial for human tissue-engineered skin substitutes: preclinical comparative in vivo study of wound healing, J. Eur. Acad. Dermatol. Venereol. 34 (2020) 2414–2427, https://doi.org/10.1111/jdv.16342.

[44] J. Riedl, C. Popp, C. Eide, J. Tolar, Mesenchymal stromal cells in wound healing applications: role of the secretome, targeted delivery and impact on recessive dystrophic epidermolysis bullosa treatment, Cytotherapy 23 (2021) 961–973, https://doi.org/10.1016/j.jcyt.2021.06.004.

[45] E. López-Ruiz, G. Jiménez, W. Kwiatkowski, E. Montañez, F. Arrebola, E. Carrillo, S. Choe, J. Marchal, M. Perán, Impact of TGF-β family-related growth factors on chondrogenic differentiation of adipose-derived stem cells isolated from lipoaspirates and infrapatellar fat pads of osteoarthritic patients, Eur. Cell. Mater. 35 (2018) 209–224, https://doi.org/10.22203/eCM.v035a15.

[46] P. Gálvez-Martín, A. Hmadcha, B. Soria, A.C. Calpena-Campmany, B. Clares-Naveros, Study of the stability of packaging and storage conditions of human mesenchymal stem cell for intra-arterial clinical application in patient with critical limb ischemia, Eur. J. Pharm. Biopharm. 86 (2014) 459–468, https://doi.org/10.1016/j.ejpb.2013.11.002.

[47] V. Carriel, I. Garzón, J.-M. Jiménez, A.-C.-X. Oliveira, S. Arias-Santiago, A. Campos, M.-C. Sánchez-Quevedo, M. Alaminos, Epithelial and stromal developmental patterns in a novel substitute of the human skin generated with fibrin-agarose biomaterials, Cells Tissues Organs 196 (2012) 1–12, https://doi.org/10.1159/000330682.

[48] R.A. Brown, M. Wiseman, C.-B. Chuo, U. Cheema, S.N. Nazhat, Ultrarapid engineering of biomimetic materials and tissues: fabrication of nano- and microstructures by plastic compression, Adv. Funct. Mater. 15 (2005) 1762–1770, https://doi.org/10.1002/adfm.200500042.

[49] G. Scionti, M. Moral, M. Toledano, R. Osorio, J.D.G. Durán, M. Alaminos, A. Campos, M.T. López-López, Effect of the hydration on the biomechanical properties in a fibrin-agarose tissue-like model, J. Biomed. Mater. Res. 102 (2014) 2573–2582, https://doi.org/10.1002/jbm.a.34929.

[50] J.L. Soriano-Ruiz, P. Gálvez-Martín, E. López-Ruiz, J. Suñer-Carbó, A.C. Calpena-Campmany, J.A. Marchal, B. Clares-Naveros, Design and evaluation of mesenchymal stem cells seeded chitosan/glycosaminoglycans quaternary hydrogel scaffolds for wound healing applications, Int J Pharm 570 (2019) 118632, https://doi.org/10.1016/j.ijpharm.2019.118632.

[51] J. Schindelin, I. Arganda-Carreras, E. Frise, V. Kaynig, M. Longair, T. Pietzsch, S. Preibisch, C. Rueden, S. Saalfeld, B. Schmid, J.-Y. Tinevez, D.J. White, V. Hartenstein, K. Eliceiri, P. Tomancak, A. Cardona, Fiji: an open-source platform for biological-image analysis, Nat. Methods 9 (2012) 676–682, https://doi.org/10.1038/nmeth.2019.

[52] C. Chocarro-Wrona, J. de Vicente, C. Antich, G. Jiménez, D. Martínez-Moreno, E. Carrillo, E. Montañez, P. Gálvez-Martín, M. Perán, E. López-Ruiz, J.A. Marchal, Validation of the 1,4-butanediol thermoplastic polyurethane as a novel material for 3D bioprinting applications, Bioeng Transl Med 6 (2021) 1–14, https://doi.org/10.1002/btm2.10192.

[53] R.S. Kellar, R.B. Diller, A.J. Tabor, D.D. Dominguez, R.G. Audet, T.A. Bardsley, A.J. Talbert, N.D. Cruz, A.L. Ingraldi, B.D. Ensley, Improved wound closure rates and mechanical properties resembling native skin in murine diabetic wounds treated with a tropoelastin and collagen wound healing device, J Diabetes Clin Res 2 (2020) 86, https://doi.org/10.33696/diabetes.1.024.

[54] L.J. Draaijers, F.R.H. Tempelman, Y.A.M. Botman, W.E. Tuinebreijer, E. Middelkoop, R.W. Kreis, P.P.M. van Zuijlen, The patient and observer scar assessment scale: a reliable and feasible tool for scar evaluation, Plast. Reconstr. Surg. 113 (2004) 1960–1965, https://doi.org/10.1097/01.PRS.0000122207.28773.56.

[55] A.L. van de Kar, L.U.M. Corion, M.J.C. Smeulders, L.J. Draaijers, C.M.A.M. van der Horst, P.P.M. van Zuijlen, Reliable and feasible evaluation of linear scars by the patient and observer scar assessment scale, Plast. Reconstr. Surg. 116 (2005) 514–522, https://doi.org/10.1097/01.prs.0000172982.43599.d6.

[56] J. Kober, A. Gugerell, M. Schmid, L.-P. Kamolz, M. Keck, Generation of a fibrin based three-layered skin substitute, BioMed Res. Int. 2015 (2015) 1–8, https://doi.org/10.1155/2015/170427.

[57] M. Konop, M. Rybka, A. Drapała, Keratin biomaterials in skin wound healing, an old player in modern medicine: a mini review, Pharmaceutics 13 (2021) 2029, https://doi.org/10.3390/pharmaceutics13122029.

[58] W.S. Choi, J.H. Kim, C.B. Ahn, J.H. Lee, Y.J. Kim, K.H. Son, J.W. Lee, Development of a multi-layer skin substitute using human hair keratinic extract-based hybrid 3D printing, Polymers 13 (2021) 2584, https://doi.org/10.3390/polym13162584.

[59] N. Bhardwaj, W.T. Sow, D. Devi, K.W. Ng, B.B. Mandal, N.-J. Cho, Silk fibroin–keratin based 3D scaffolds as a dermal substitute for skin tissue engineering, Integr. Biol. 7 (2015) 53–63, https://doi.org/10.1039/C4IB00208C.

[60] J. Navarro, R.M. Clohessy, R.C. Holder, A.R. Gabard, G.J. Herendeen, R.J. Christy, L.R. Burnett, J.P. Fisher, In vivo evaluation of three-dimensional printed, keratin-based hydrogels in a porcine thermal burn model, Tissue Eng Part A 26 (2020) 265–278, https://doi.org/10.1089/ten.tea.2019.0181.

[61] F.F. Schmidt, S. Nowakowski, P.J. Kluger, Improvement of a three-layered in vitro skin model for topical application of irritating substances, Front. Bioeng. Biotechnol. 8 (2020) 528082, https://doi.org/10.3389/fbioe.2020.00388.

[62] M. Rahimnejad, T. Labonté-Dupuis, N.R. Demarquette, S. Lerouge, A rheological approach to assess the printability of thermosensitive chitosan-based biomaterial inks, Biomedical Materials 16 (2021) 015003, https://doi.org/10.1088/1748-605X/abb2d8.

[63] A. Schwab, R. Levato, M. D'Este, S. Piluso, D. Eglin, J. Malda, Printability and shape fidelity of bioinks in 3D bioprinting, Chem Rev 120 (2020) 11028–11055, https://doi.org/10.1021/acs.chemrev.0c00084.

[64] A. Ciszek, Variability of skin pH after the use of different collagen gels, J. Cosmet. Dermatol. 16 (2017) 531–536, https://doi.org/10.1111/jocd.12303.

[65] Y. Gao, W. Kong, B. Li, Y. Ni, T. Yuan, L. Guo, H. Lin, H. Fan, Y. Fan, X. Zhang, Fabrication and characterization of collagen-based injectable and self-crosslinkable hydrogels for cell encapsulation, Colloids Surf. B Biointerfaces 167 (2018) 448–456, https://doi.org/10.1016/j.colsurfb.2018.04.009.

[66] N. Bhattarai, J. Gunn, M. Zhang, Chitosan-based hydrogels for controlled, localized drug delivery, Adv. Drug Deliv. Rev. 62 (2010) 83–99, https://doi.org/10.1016/j.addr.2009.07.019.

[67] E. Mancha Sánchez, J.C. Gómez-Blanco, E. López Nieto, J.G. Casado, A. Macías-García, M.A. Díaz Díez, J.P. Carrasco-Amador, D. Torrejón Martín, F.M. Sánchez-Margallo, J.B. Pagador, Hydrogels for bioprinting: a systematic review of hydrogels synthesis, bioprinting parameters, and bioprinted structures behavior, Front. Bioeng. Biotechnol. 8 (2020) 541593, https://doi.org/10.3389/fbioe.2020.00776.

[68] C. Ceccaldi, E. Assaad, E. Hui, M. Buccionyte, A. Adoungotchodo, S. Lerouge, Optimization of injectable thermosensitive scaffolds with enhanced mechanical properties for cell therapy, Macromol. Biosci. 17 (2017) 1600435, https://doi.org/10.1002/mabi.201600435.

[69] J. Jachowicz, R. McMullen, D. Prettypaul, Indentometric analysis of in vivo skin and comparison with artificial skin models, Skin Res. Technol. 13 (2007) 299–309, https://doi.org/10.1111/j.1600-0846.2007.00229.x.

[70] J. Liu, H. Zheng, P. Poh, H.-G. Machens, A. Schilling, Hydrogels for engineering of perfusable vascular networks, Int. J. Mol. Sci. 16 (2015) 15997–16016, https://doi.org/10.3390/ijms160715997.

[71] A. Kalra, A. Lowe, A.-J. Am, Mechanical behaviour of skin: a review, J Material Sci Eng 5 (2016) 4, https://doi.org/10.4172/2169-0022.1000254.

[72] J.J. Egea-Guerrero, G. Carmona, E. Correa, R. Mata, S. Arias-Santiago, M. Alaminos, P. Gacto, N. Cuende, Transplant of tissue-engineered artificial autologous human skin in Andalusia: an example of coordination and institutional collaboration, Transplant. Proc. 51 (2019) 3047–3050, https://doi.org/10.1016/j.transproceed.2019.08.014.

[73] N. Ferrara, Vascular endothelial growth factor: basic science and clinical progress, Endocr. Rev. 25 (2004) 581–611, https://doi.org/10.1210/er.2003-0027.

[74] M.G. Tonnesen, X. Feng, R.A.F. Clark, Angiogenesis in wound healing, J. Invest. Dermatol. Symp. Proc. 5 (2000) 40–46, https://doi.org/10.1046/j.1087-0024.2000.00014.x.

[75] S. Werner, R. Grose, Regulation of wound healing by growth factors and cytokines, Physiol. Rev. 83 (2003) 835–870, https://doi.org/10.1152/physrev.2003.83.3.835.

[76] D.M. Ornitz, N. Itoh, Fibroblast growth factors, Genome Biol. 2 (2001), https://doi.org/10.1186/GB-2001-2-3-REVIEWS3005 reviews3005.1.

[77] L.W. Fui, M.P.W. Lok, V. Govindasamy, T.K. Yong, T.K. Lek, A.K. Das, Understanding the multifaceted mechanisms of diabetic wound healing and therapeutic application of stem cells conditioned medium in the healing process, J Tissue Eng Regen Med 13 (2019) 2218–2233, https://doi.org/10.1002/term.2966.

[78] R. Baserga, The insulin-like growth factor I receptor: a key to tumor growth? Cancer Res. 55 (1995) 249–252.

[79] J.I. Jones, D.R. Clemmons, Insulin-like growth factors and their binding proteins: biological actions, Endocr. Rev. 16 (1995) 3–34, https://doi.org/10.1210/edrv-16-1-3.

[80] G. Vardatsikos, A. Sahu, A.K. Srivastava, The insulin-like growth factor family: molecular mechanisms, redox regulation, and clinical implications, Antioxid Redox Signal 11 (2009) 1165–1190, https://doi.org/10.1089/ars.2008.2161.

[81] B. Hempstead, Dissecting the diverse actions of pro- and mature neurotrophins, Curr. Alzheimer Res. 3 (2006) 19–24, https://doi.org/10.2174/156720506775697061.

[82] S. Gordon, Alternative activation of macrophages, Nat. Rev. Immunol. 3 (2003) 23–35, https://doi.org/10.1038/nri978.

[83] F. Truzzi, A. Marconi, C. Pincelli, Neurotrophins in healthy and diseased skin, Dermatoendocrinol 3 (2011) 32–36, https://doi.org/10.4161/derm.3.1.14661.

[84] V.A. Botchkarev, M. Yaar, E.M.J. Peters, S.P. Raychaudhuri, N.V. Botchkareva, A. Marconi, S.K. Raychaudhuri, R. Paus, C. Pincelli, Neurotrophins in skin biology and pathology, J. Invest. Dermatol. 126 (2006) 1719–1727, https://doi.org/10.1038/sj.jid.5700270.

[85] R.A.F. Clark, The Molecular and Cellular Biology of Wound Repair, second ed., Springer US, Boston, MA, 1988 https://doi.org/10.1007/978-1-4899-0185-9.

[86] P. Chandrasoma, C.R. Taylor, Chapter 6. Healing & repair, in: Concise Pathology, third ed., McGraw Hill, 1998. https://accessphysiotherapy.mhmedical.com/content.aspx?bookid=333&sectionid=40013178.

[87] Y. Zhang, D. Li, S. Fang, X. Li, H. Zhang, H. Dai, H. Fan, Y. Li, D. Shen, W. Tang, C. Yang, X. Xing, Stimulatory effect of engineered three-layer adipose tissue-derived stem cells sheet in atelocollagen matrix on wound healing in a mouse model of radiation-induced skin injury, J. Biomater. Appl. 34 (2019) 498–508, https://doi.org/10.1177/0885328219862123.

[88] L.E. Tracy, R.A. Minasian, E.J. Caterson, Extracellular matrix and dermal fibroblast function in the healing wound, Adv. Wound Care 5 (2016) 119–136, https://doi.org/10.1089/wound.2014.0561.

[89] J. Melrose, Glycosaminoglycans in wound healing, Bone Tissue Regen. Insights 7 (2016), https://doi.org/10.4137/BTRI.S38670. BTRI.S38670.

[90] Q. Xu, J.E. Torres, M. Hakim, P.M. Babiak, P. Pal, C.M. Battistoni, M. Nguyen, A. Panitch, L. Solorio, J.C. Liu, Collagen- and hyaluronic acid-based hydrogels and their biomedical applications, Mater. Sci. Eng. R Rep. 146 (2021) 100641, https://doi.org/10.1016/j.mser.2021.100641.

[91] L. Gardeazabal, A. Izeta, Elastin and collagen fibres in cutaneous wound healing, Exp. Dermatol. 33 (2024), https://doi.org/10.1111/exd.15052.

[92] V. Sarangthem, T.D. Singh, A.K. Dinda, Emerging role of elastin-like polypeptides in regenerative medicine, Adv. Wound Care 10 (2021) 257–269, https://doi.org/10.1089/wound.2019.1085.

[93] D.-M. Tian, H.-H. Wan, J.-R. Chen, Y.-B. Ye, Y. He, Y. Liu, L.-Y. Tang, Z.-Y. He, K.-Z. Liu, C.-J. Gao, S.-L. Li, Q. Xu, Z. Yang, C. Lai, X.-J. Xu, C.-S. Ruan, Y.-S. Xu, C. Zhang, L. Luo, L.-P. Yan, In-situ formed elastin-based hydrogels enhance wound healing via promoting innate immune cells recruitment and angiogenesis, Mater Today Bio 15 (2022) 100300, https://doi.org/10.1016/j.mtbio.2022.100300.

[94] J.C. Rodríguez-Cabello, I. González de Torre, A. Ibañez-Fonseca, M. Alonso, Bioactive scaffolds based on elastin-like materials for wound healing, Adv. Drug Deliv. Rev. 129 (2018) 118–133, https://doi.org/10.1016/j.addr.2018.03.003.

[95] S.M. Staubli, G. Cerino, I. Gonzalez De Torre, M. Alonso, D. Oertli, F. Eckstein, K. Glatz, J.C. Rodríguez Cabello, A. Marsano, Control of angiogenesis and host response by modulating the cell adhesion properties of an Elastin-Like Recombinamer-based hydrogel, Biomaterials 135 (2017) 30–41, https://doi.org/10.1016/j.biomaterials.2017.04.047.

[96] A. Pirayesh, H. Hoeksema, C. Richters, J. Verbelen, S. Monstrey, Glyaderm® dermal substitute: clinical application and long-term results in 55 patients, Burns 41 (2015) 132–144, https://doi.org/10.1016/j.burns.2014.05.013.

[97] N. Annabi, S.M. Mithieux, E.A. Boughton, A.J. Ruys, A.S. Weiss, F. Dehghani, Synthesis of highly porous crosslinked elastin hydrogels and their interaction with fibroblasts in vitro, Biomaterials 30 (2009) 4550–4557, https://doi.org/10.1016/j.biomaterials.2009.05.014.

[98] D. Wang, J. Zeng, H. Zhu, S. Liu, L. Jia, W. Liu, Q. Wang, S. Wang, W. Liu, J. Zhou, H. Chen, X. Liu, H. Jiang, Extrusion bioprinting of elastin-containing bioactive double-network tough hydrogels for complex elastic tissue regeneration, Aggregate 5 (2024) e477, https://doi.org/10.1002/agt2.477.

[99] S. Werner, T. Krieg, H. Smola, Keratinocyte–fibroblast interactions in wound healing, J. Invest. Dermatol. 127 (2007) 998–1008, https://doi.org/10.1038/sj.jid.5700786.

[100] M. Mahjoor, A. Fakouri, S. Farokhi, H. Nazari, H. Afkhami, F. Heidari, Regenerative potential of mesenchymal stromal cells in wound healing: unveiling the influence of normoxic and hypoxic environments, Front. Cell Dev. Biol. 11 (2023), https://doi.org/10.3389/fcell.2023.1245872.

[101] D. Tsuruta, K.J. Green, S. Getsios, J.C.R. Jones, The barrier function of skin: how to keep a tight lid on water loss, Trends Cell Biol. 12 (2002) 355–357, https://doi.org/10.1016/S0962-8924(02)02316-4.

[102] M. Akdeniz, S. Gabriel, A. Lichterfeld-Kottner, U. Blume-Peytavi, J. Kottner, Transepidermal water loss in healthy adults: a systematic review and meta-analysis update, Br. J. Dermatol. 179 (2018) 1049–1055, https://doi.org/10.1111/bjd.17025.

[103] K.-H. Busch, A. Aliu, N. Walezko, M. Aust, Medical needling: effect on moisture and transepidermal water loss of mature hypertrophic burn scars, Cureus 10 (2018), https://doi.org/10.7759/cureus.2365.

[104] D. Maroto-Morales, T. Montero-Vilchez, S. Arias-Santiago, Study of skin barrier function in psoriasis: the impact of emollients, Life 11 (2021) 651, https://doi.org/10.3390/life11070651.

[105] L. Baumann, E.F. Bernstein, A.S. Weiss, D. Bates, S. Humphrey, M. Silberberg, R. Daniels, Clinical relevance of elastin in the structure and function of skin, Aesthet Surg J Open Forum 3 (2021), https://doi.org/10.1093/asjof/ojab019.

[106] S. Hauck, P. Zager, N. Halfter, E. Wandel, M. Torregrossa, A. Kakpenova, S. Rother, M. Ordieres, S. Räthel, A. Berg, S. Möller, M. Schnabelrauch, J.

C. Simon, V. Hintze, S. Franz, Collagen/hyaluronan based hydrogels releasing sulfated hyaluronan improve dermal wound healing in diabetic mice via reducing inflammatory macrophage activity, Bioact. Mater. 6 (2021) 4342–4359, https://doi.org/10.1016/j.bioactmat.2021.04.026.

[107] K. Valachová, L. Šoltés, Hyaluronan as a prominent biomolecule with numerous applications in medicine, Int. J. Mol. Sci. 22 (2021) 7077, https://doi.org/10.3390/ijms22137077.

[108] M. Brenner, V.J. Hearing, The protective role of melanin against UV damage in human skin, Photochem. Photobiol. 84 (2008) 539–549, https://doi.org/10.1111/j.1751-1097.2007.00226.x.

[109] S. Chadwick, R. Heath, M. Shah, Abnormal pigmentation within cutaneous scars: a complication of wound healing, Indian J. Plast. Surg. 45 (2012) 403–411, https://doi.org/10.4103/0970-0358.101328.

[110] S. Tsukada, The melanocytes and melanin in human skin autografts, Plast. Reconstr. Surg. 53 (1974) 200–207, https://doi.org/10.1097/00006534-197402000-00012.

[111] M.T. Cerqueira, R.P. Pirraco, A.R. Martins, T.C. Santos, R.L. Reis, A.P. Marques, Cell sheet technology-driven re-epithelialization and neovascularization of skin wounds, Acta Biomater. 10 (2014) 3145–3155, https://doi.org/10.1016/j.actbio.2014.03.006.

[112] M. Kallioinen, V. Koivukangas, M. Jarvinen, A. Oikarinen, Expression of cytokeratins in regenerating human epidermis, Br. J. Dermatol. 133 (1995) 830–835, https://doi.org/10.1111/j.1365-2133.1995.tb06912.x.

[113] J. Patten, K. Wang, Fibronectin in development and wound healing, Adv. Drug Deliv. Rev. 170 (2021) 353–368, https://doi.org/10.1016/j.addr.2020.09.005.

[114] M.A. Ambele, P. Dhanraj, R. Giles, M.S. Pepper, Adipogenesis: a complex interplay of multiple molecular determinants and pathways, Int. J. Mol. Sci. 21 (2020) 4283, https://doi.org/10.3390/ijms21124283.

[115] G. Rivera-Gonzalez, B. Shook, V. Horsley, Adipocytes in skin Health and disease, Cold Spring Harb Perspect Med 4 (2014), https://doi.org/10.1101/cshperspect.a015271-a015271.

[116] M. Liu, F. Lu, J. Feng, Aging and homeostasis of the hypodermis in the age-related deterioration of skin function, Cell Death Dis. 15 (2024) 443, https://doi.org/10.1038/s41419-024-06818-z.

[117] G.J. Hausman, D.R. Campion, R.L. Richardson, R.J. Martin, Adipocyte development in the rat hypodermis, Am. J. Anat. 161 (1981) 85–100, https://doi.org/10.1002/aja.1001610107.

[118] D. Park, Y. Kim, H. Kim, K. Kim, Y.-S. Lee, J. Choe, J.-H. Hahn, H. Lee, J. Jeon, C. Choi, Y.-M. Kim, D. Jeoung, Hyaluronic acid promotes angiogenesis by inducing RHAMM-tgfβ receptor interaction via CD44-PKCδ, Mol. Cells 33 (2012) 563–574, https://doi.org/10.1007/s10059-012-2294-1.

[119] Y. Luo, F. Liang, X. Wan, S. Liu, L. Fu, J. Mo, X. Meng, Z. Mo, Hyaluronic acid facilitates angiogenesis of endothelial Colony forming cell combining with mesenchymal stem cell via CD44/MicroRNA-139-5p pathway, Front. Bioeng. Biotechnol. 10 (2022) 794037, https://doi.org/10.3389/fbioe.2022.794037.

[120] D. Béchard, T. Gentina, M. Delehedde, A. Scherpereel, M. Lyon, M. Aumercier, R. Vazeux, C. Richet, P. Degand, B. Jude, A. Janin, D.G. Fernig, A.-B. Tonnel, P. Lassalle, Endocan is a novel chondroitin sulfate/dermatan sulfate proteoglycan that promotes hepatocyte growth factor/scatter factor mitogenic activity, J. Biol. Chem. 276 (2001) 48341–48349, https://doi.org/10.1074/jbc.M108395200.

[121] P.T. Thevenot, A.M. Nair, J. Shen, P. Lotfi, C.-Y. Ko, L. Tang, The effect of incorporation of SDF-1α into PLGA scaffolds on stem cell recruitment and the inflammatory response, Biomaterials 31 (2010) 3997–4008, https://doi.org/10.1016/j.biomaterials.2010.01.144.

[122] A. Ridiandries, J.T.M. Tan, C.A. Bursill, The role of chemokines in wound healing, Int. J. Mol. Sci. 19 (2018) 3217, https://doi.org/10.3390/ijms19103217.

[123] M.N. Ajuebor, C.M. Hogaboam, S.L. Kunkel, A.E.I. Proudfoot, J.L. Wallace, The chemokine RANTES is a crucial mediator of the progression from acute to chronic colitis in the rat, J. Immunol. 166 (2001) 552–558, https://doi.org/10.4049/jimmunol.166.1.552.

[124] F. Zamboni, S. Vieira, R.L. Reis, J. Miguel Oliveira, M.N. Collins, The potential of hyaluronic acid in immunoprotection and immunomodulation: chemistry, processing and function, Prog. Mater. Sci. 97 (2018) 97–122, https://doi.org/10.1016/j.pmatsci.2018.04.003.

[125] M. Kharaziha, A. Baidya, N. Annabi, Rational Design of immunomodulatory hydrogels for chronic wound healing, Adv. Mater. 33 (2021), https://doi.org/10.1002/adma.202100176.

[126] T. Yuan, L. Zhang, K. Li, H. Fan, Y. Fan, J. Liang, X. Zhang, Collagen hydrogel as an immunomodulatory scaffold in cartilage tissue engineering, J. Biomed. Mater. Res. B Appl. Biomater. 102 (2014) 337–344, https://doi.org/10.1002/jbm.b.33011.

[127] S.G. Llames, M. Del Rio, F. Larcher, E. García, M. García, M. José Escamez, J. L. Jorcano, P. Holguín, A. Meana, Human plasma as a dermal scaffold for the generation of a completely autologous bioengineered skin, Transplantation 77 (2004) 350–355, https://doi.org/10.1097/01.TP.0000112381.80964.85.

[128] S. Llames, E. García, V. García, M. del Río, F. Larcher, J.L. Jorcano, E. López, P. Holguín, F. Miralles, J. Otero, A. Meana, Clinical results of an autologous engineered skin, Cell Tissue Bank. 7 (2006) 47–53, https://doi.org/10.1007/s10561-004-7253-4.

[129] F. Kawecki, D. Mayrand, A. Ayoub, E. Attiogbe, L. Germain, F.A. Auger, V. J. Moulin, Biofabrication and preclinical evaluation of a large-sized human self-assembled skin substitute, Biomedical Materials 16 (2020) 025023, https://doi.org/10.1088/1748-605X/abbdbe.